

Latent Correlation-Based Multiview Learning and Self-Supervision: A Unifying Perspective

Qi Lyu*, Xiao Fu*, Weiran Wang[‡], and Songtao Lu[†]

*School of Electrical Engineering and Computer Science
Oregon State University,
Corvallis, OR 97331, United States
Email: {lyuqi, xiao.fu}@oregonstate.edu

[‡]Google Inc.
Mountain View, CA 94043, United States
Email: weiranwang@ttic.edu

[†]IBM Watson
Yorktown Heights, NY 10598, United States
Email: songtao@ibm.com

Abstract

Multiple views of data, both naturally acquired (e.g., image and audio) and artificially produced (e.g., via adding different noise to data samples), have proven useful in enhancing representation learning. Natural views are often handled by multiview analysis tools, e.g., (deep) canonical correlation analysis [(D)CCA], while the artificial ones are frequently used in self-supervised learning (SSL) paradigms, e.g., *SimCLR* and *Barlow Twins*. Both types of approaches often involve learning neural feature extractors such that the embeddings of data exhibit high cross-view correlations. Although intuitive, the effectiveness of correlation-based neural embedding is only empirically validated. This work puts forth a theory-backed framework for unsupervised multiview learning. Our development starts with proposing a multiview model, where each view is a nonlinear mixture of shared and private components. Consequently, the learning problem boils down to shared/private component identification and disentanglement. Under this model, latent correlation maximization is shown to guarantee the extraction of the shared components across views (up to certain ambiguities). In addition, the private information in each view can be provably disentangled from the shared using proper regularization design. The method is tested on a series of tasks, e.g., downstream clustering, which all show promising performance. Our development also provides a unifying perspective for understanding various DCCA and SSL schemes.

1 Introduction

Unsupervised representation learning (URL)—e.g., principal component analysis (PCA), nonnegative matrix factorization (NMF), and independent component analysis (ICA)—lies at the heart of dimensionality reduction (DR). In the era of deep learning (DL), many new paradigms have shown potentials, e.g., deep autoencoder (DAE) [1], contrastive learning [2, 3], and more recently, self-supervised learning (SSL) [4–8]. **From CCA to Deep CCA.** One pillar of URL is multiview representation learning. Extracting shared information from multiple “views” (e.g., image and audio) of data entities has been considered a major

means to fend against noise and data scarcity. Critical analytical tools include *canonical correlation analysis* (CCA) [9], tensor decomposition [10], and partial least squares (PLS) [11]. Among others, CCA is particularly appealing due to its robustness to strong private (i.e., view-specific) interference [12, 13]. However, the classic CCA seeks linear transformation matrices such that transformed views are maximally correlated—but linear transformations have limited expressive power. A number of works studied nonlinear extensions of CCA; see kernel CCA in [14] and deep learning-based CCA (DCCA) in [15, 16]. In particular, DCCA and its variants were shown to largely outperform the classical linear CCA in a number of tasks [15, 16].

Artificial Views and SSL. In recent years, a series of SSL paradigms were proposed to artificially *distort* data—e.g., by rotating, cropping, and/or adding noise to data samples—to create different views [4–6, 17]. Then, neural encoders are employed to map these artificial views to embeddings that are highly correlated across views. The idea is intuitive: essential information of data should be invariant to distortions. This genre—which will be referred to as artificial multiview SSL (AM-SSL)—includes many frameworks, e.g., SimCLR [4], BYOL [17], SimSiam [18], and Barlow Twins [19].

Latent Correlation Maximization. Both the DCCA-type approaches [15, 16, 20, 21] and many AM-SSL approaches [3, 4, 17–19] seek maximally correlated representations from multiple views, using neural networks as view-specific feature extractors (encoders). The successes of DCCA and AM-SSL bears an important research question: How to understand the effectiveness of cross-view correlation-related learning criteria? Furthermore, how to use such understanding to design theory-backed learning criteria to serve various purposes, e.g., shared and/or private information extraction?

1.1 Contributions

We aim at providing a latent correlation-based multiview learning framework with provable guarantees. Our detailed contributions lie in the following aspects:

Learning Framework Design. We start with modeling multiple views of data as *unknown* nonlinear mixtures of shared and private latent components. This way, the objective of multiview learning boils down to extracting the shared and private information, respectively. Based on this perspective, we propose a learning criterion that maximizes the correlation of the shared part extracted from different views, while minimizing the dependence between the private components and shared components.

Identifiability Analysis. With the designed criterion, we show that the shared and private components in different views can be provably identified up to certain ambiguities. Our result sheds new light onto the effectiveness of latent correlation analysis, and articulates the importance of imposing model/problem-specific regularization—which are consistent with the experience gained from DCCA and AM-SSL research. Notably, on top of learning the shared information, our framework also guarantees the extraction of the private information of each view. Learning private information has been less addressed in DCCA and AM-SSL—let alone provable guarantees—but is useful in many applications, e.g., cross-view data generation. Moreover, we provide sample complexity analysis for our learning framework, which is the first of its kind, to our best knowledge.

Practical Implementation. To realize our learning criterion, we design a regularized deep multiview learning neural architecture. Our network structure bears interesting resemblances to DCCA and AM-SSL methods (in particular, deep canonically correlated autoencoders (DCCAE) [16] and Barlow Twins [19]), while admits critical differences that entail the desired identifiability guarantees. A notable innovation is a minimax deep correlation-based group independence-regularizer, which shares the same purpose of some known independence promoters (e.g., *Hilbert-Schmidt Information Criterion* (HSIC) [22]) but is arguably easier to implement using stochastic gradient algorithms.

We test our method on various tasks involving natural and artificial multiview data, and the results corroborate our design goals and theoretical analyses.

Notation. The notations used in this work are summarized in the supplementary material.

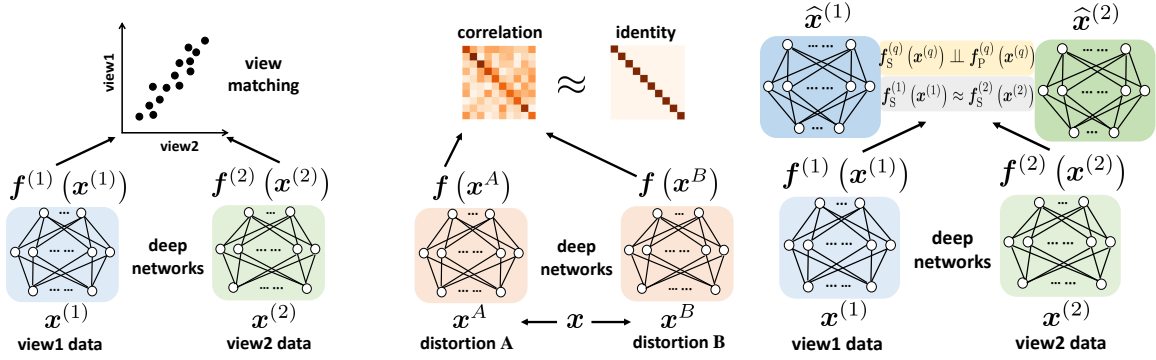


Figure 1: From left to right: DCCA [15,16], Barlow Twins [19] and the proposed.

2 Background: Deep CCA and Self-Supervision

Multiview Analysis and DCCA. Extracting essential shared information from multiple views has been a long existing topic. In particular, CCA [9,23] and its variants like DCCA [15,16] learn embeddings of data entities via maximizing the correlation of low-dimensional representations extracted from multiple feature domains (i.e., views) using linear and neural encoders, respectively. The objective of DCCA can be summarized as follows: [15]:

$$\underset{\mathbf{f}^{(1)}, \mathbf{f}^{(2)}}{\text{maximize}} \text{Tr} \left(\mathbb{E} \left[\mathbf{f}^{(1)}(\mathbf{x}^{(1)}) \mathbf{f}^{(2)}(\mathbf{x}^{(2)})^\top \right] \right), \quad \text{s.t.} \mathbb{E} \left[\mathbf{f}^{(q)}(\mathbf{x}^{(q)}) \mathbf{f}^{(q)}(\mathbf{x}^{(q)})^\top \right] = \mathbf{I}, \quad (1)$$

where $\mathbf{x}^{(q)} \in \mathbb{R}^{M_q} \sim \mathcal{D}_q$ is a data sample from view q for $q = 1, 2$, \mathcal{D}_q is the underlying distribution of the q th view, $\mathbf{f}^{(1)} : \mathbb{R}^{M_1} \rightarrow \mathbb{R}^D$ and $\mathbf{f}^{(2)} : \mathbb{R}^{M_2} \rightarrow \mathbb{R}^D$ are two neural networks; see Fig. 1. CCA was found particularly useful in terms of fending against unknown and strong view-specific (private) interference (see theoretical supports in [12,13]). Such properties were also observed in DCCA research [16], while theoretical analysis is mostly elusive.

Artificial Multiviews and SSL. The goal of AM-SSL is to find distortion-invariant deep encoders. The idea is often realized via intentionally distorting the data samples to create multiple artificial views. Then, the encoders are required to produce highly correlated embeddings from such views. Many of these methods, e.g., SimCLR [4], BYOL [17], and SimSiam [18] use different neural network structures and negative sampling schemes to assist latent correlation maximization, in order to avoid trivial solutions and improve performance.

The most recent development, namely, the Barlow Twins network [19] is appealing since it entails a succinct implementation. Specifically, the Barlow Twins network aims to learn a *single* encoder $\mathbf{f} : \mathbb{R}^M \rightarrow \mathbb{R}^D$ for two distorted views, denoted as $\mathbf{x}^A \in \mathbb{R}^M$ and $\mathbf{x}^B \in \mathbb{R}^M$ with $\mathbf{z}^A = \mathbf{f}(\mathbf{x}^A)$ and $\mathbf{z}^B = \mathbf{f}(\mathbf{x}^B)$. The cost function minimizes $\sum_{i=1}^D (1 - C_{ii})^2 + \lambda \sum_{i=1}^D \sum_{j \neq i}^D C_{ij}^2$, where $C_{ij} = \mathbb{E}[z_i^A z_j^B] / (\sqrt{\mathbb{E}[(z_i^A)^2]} \sqrt{\mathbb{E}[(z_j^B)^2]})$ is the cross-correlation between z_i^A and z_j^B , the learned embeddings $\mathbf{z}^A, \mathbf{z}^B$ are constrained to have zero mean, i.e., $\mathbb{E}[\mathbf{z}^A] = \mathbb{E}[\mathbf{z}^B] = \mathbf{0}$; see Fig. 1.

3 Proposed Framework

In this work, we offer a unifying perspective for multiview analysis, from a shared and private information extraction view point.

3.1 Multiview as Nonlinear Mixtures of Private and Shared Components

We consider the following multiview generative model:

$$\mathbf{x}_\ell^{(1)} = \mathbf{g}^{(1)} \left(\begin{bmatrix} \mathbf{z}_\ell \\ \mathbf{c}_\ell^{(1)} \end{bmatrix} \right), \quad \mathbf{x}_\ell^{(2)} = \mathbf{g}^{(2)} \left(\begin{bmatrix} \mathbf{z}_\ell \\ \mathbf{c}_\ell^{(2)} \end{bmatrix} \right), \quad (2)$$

where $\mathbf{x}_\ell^{(q)} \in \mathbb{R}^{M_q}$ is the ℓ th sample of the q th view for $q = 1, 2$, $\mathbf{z}_\ell \in \mathbb{R}^D$ is the shared component across views, and $\mathbf{c}_\ell^{(q)} \in \mathbb{R}^{D_q}$ represents the private information of the q th view—which are the ℓ th samples of continuous random variables denoted by $\mathbf{z} \in \mathbb{R}^D$, $\mathbf{c}^{(q)} \in \mathbb{R}^{D_q}$, respectively. In addition, $\mathbf{g}^{(q)}(\cdot) : \mathbb{R}^{D+D_q} \rightarrow \mathbb{R}^{M_q}$ is an *invertible* and *smooth* nonlinear transformation, which is unknown.

Note that (2) can be understood as a nonlinear generalization of the linear CCA models in [12, 13], where two views of data are *linear transformations* of shared latent components with private interference terms. Particularly, in [13], the views are modeled as $\mathbf{x}_\ell^{(q)} = \mathbf{A}^{(q)}[\mathbf{z}_\ell^\top, (\mathbf{c}_\ell^{(q)})^\top]^\top$ for $q = 1, 2$. This type of modeling may be helpful in understanding several interesting aspects:

Denoised Embedding. A key takeaway in the linear CCA works is that latent correlation maximization can provably extract the shared information—under strong and unknown private noise [12, 13]. If this perspective is also carried over to the more general case in (2), it may provide important support/justification to DCCA type approaches.

Distortion-Invariant Learning. The model in (2) is also suitable for interpreting the effectiveness of AM-SSL. To be specific, if one views $\mathbf{g}^{(q)}(\cdot)$ and $\mathbf{c}^{(q)}$ as the artificial distortions that are responsible for creating the q th view, then extracting distortion-invariant information (as AM-SSL paradigms aspire to) boils down to extracting \mathbf{z} 's information.

Private Information Learning. We should remark that modeling and learning the private information represented by $\mathbf{c}^{(q)}$ (or its transformations) is also important in applications like cross-view data generation (e.g., image translation [24, 25]).

Objective and Challenge. Under the model in (2), our goal is to disentangle the shared \mathbf{z} and the private information $\mathbf{c}^{(q)}$ for $q = 1, 2$ —with provable guarantees. This boils down to a nonlinear latent component identification problem with disentanglement requirements—which are in general ill-posed [26]. The developments in DCCA and AM-SSL seem to suggest that latent correlation maximization could be a viable route for shared information extraction, yet theoretical supports have been elusive. In addition, it is unclear if correlation maximization alone suffices to disentangle private and shared information.

3.2 The Proposed Learning Criterion

Given observations from both views $\{\mathbf{x}_\ell^{(1)}, \mathbf{x}_\ell^{(2)}\}_{\ell=1}^N$ generated from (2), we aim to extract the shared and private components simultaneously. In specific, consider the following problem:

$$\underset{\mathbf{f}^{(1)}, \mathbf{f}^{(2)}}{\text{maximize}} \quad \text{Tr} \left(\frac{1}{N} \sum_{\ell=1}^N \mathbf{f}_S^{(1)}(\mathbf{x}_\ell^{(1)}) \mathbf{f}_S^{(2)}(\mathbf{x}_\ell^{(2)})^\top \right) \quad (3a)$$

$$\text{subject to } \mathbf{f}^{(q)} \text{ for } q = 1, 2 \text{ are invertible,} \quad (3b)$$

$$\frac{1}{N} \sum_{\ell=1}^N \mathbf{f}_S^{(q)}(\mathbf{x}_\ell^{(q)}) \mathbf{f}_S^{(q)}(\mathbf{x}_\ell^{(q)})^\top = \mathbf{I}, \quad \frac{1}{N} \sum_{\ell=1}^N \mathbf{f}_S^{(q)}(\mathbf{x}_\ell^{(q)}) = \mathbf{0}, \quad q = 1, 2, \quad (3c)$$

$$\mathbf{f}_S^{(q)}(\mathbf{x}_\ell^{(q)}) \perp \mathbf{f}_P^{(q)}(\mathbf{x}_\ell^{(q)}), \quad q = 1, 2, \quad (3d)$$

where $\mathbf{f}^{(q)} : \mathbb{R}^{M_q} \rightarrow \mathbb{R}^{D+D_q}$ for $q = 1, 2$ are the feature extractors of view q . We use the notation

$$\mathbf{f}_S^{(q)}(\mathbf{x}_\ell^{(q)}) = \left[\mathbf{f}^{(q)}(\mathbf{x}_\ell^{(q)}) \right]_{1:D}, \quad \mathbf{f}_P^{(q)}(\mathbf{x}_\ell^{(q)}) = \left[\mathbf{f}^{(q)}(\mathbf{x}_\ell^{(q)}) \right]_{D+1:D+D_q}, \quad q = 1, 2,$$

to denote the encoder-extracted shared and private components for each view, respectively. Note that designating the first D dimensions of the encoder outputs to represent the shared information is without loss of generality, since the permutation ambiguity is intrinsic.

To explain the criterion, note that we have a couple of goals that we hope to achieve with $\mathbf{f}_S^{(q)}$ and $\mathbf{f}_P^{(q)}$. First, the objective function aims to maximize the latent correlation of the learned shared components, i.e., $\mathbf{f}_S^{(q)}$. This is similar to those in DCCA and AM-SSL, and is based on the belief that the shared information should be identical across views. Second, in (3d), we ask $\mathbf{f}_S^{(q)}$ and $\mathbf{f}_P^{(q)}$ to be statistically independent for $q = 1, 2$. This promotes the disentanglement of the shared and private parts of each encoder. View-specific components are often considered as interference or noise, both in DCCA and AM-SSL, and thus being independent to the essential information. Third, the invertibility constraint in (3b) is to ensure that the latent and the ambient data can be constructed from each other—which is often important in unsupervised learning, for avoiding trivial solutions. The orthogonality and zero-mean constraints in (3c) are used to make the correlation metric meaningful. In particular, if the learned components are not zero-mean, the learned embeddings may not capture “co-variations” but dominated by some constant terms; see [27] for discussions.

3.3 Theoretical Aspects

In this subsection, we analyze a number of theoretical aspects related to our model in (2) and learning criterion in (3). To proceed, we make the following assumption:

Assumption 1 (Group Independence) *Under (2), the samples \mathbf{z}_ℓ and $\mathbf{c}_\ell^{(q)}$ are realizations of shared and private continuous latent random variables \mathbf{z} , $\mathbf{c}^{(q)}$ for $q = 1, 2$, whose joint distributions satisfy the following:*

$$\mathbf{z} \sim p(\mathbf{z}), \mathbf{c}^{(q)} \sim p(\mathbf{c}^{(q)}), \mathbf{z} \in \mathcal{Z}, \mathbf{c}^{(q)} \in \mathcal{C}_q, p(\mathbf{z}, \mathbf{c}^{(1)}, \mathbf{c}^{(2)}) = p(\mathbf{z})p(\mathbf{c}^{(1)})p(\mathbf{c}^{(2)}), \quad (4)$$

where $\mathcal{Z} \subseteq \mathbb{R}^D$, $\mathcal{C}_q \subseteq \mathbb{R}^{D_q}$ are the continuous supports of $p(\mathbf{z})$ and $p(\mathbf{c}^{(q)})$, respectively.

We have the following theorem in terms of learning the shared and private components:

Theorem 1 *Under the generative model in (2) and Assumption 1, consider the population form in (3) (i.e., $N = \infty$). Assume that the considered constraints hold over all $\mathbf{x}^{(q)} \in \mathcal{X}_q$ for $q = 1, 2$, where $\mathcal{X}_q = \{\mathbf{x}^{(q)} | \mathbf{x}^{(q)} = \mathbf{g}^{(q)}([\mathbf{z}^\top, (\mathbf{c}^{(q)})^\top]^\top), \forall \mathbf{z} \in \mathcal{Z}, \forall \mathbf{c}^{(q)} \in \mathcal{C}_q\}$. Denote $\hat{\mathbf{f}}^{(q)}$ as any solution of (3). Also assume that the first-order derivative of $\hat{\mathbf{f}}^{(q)} \circ \mathbf{g}^{(q)}$ exists. Then, we have*

- (i) $\hat{\mathbf{z}} = \hat{\mathbf{f}}_S^{(q)}(\mathbf{x}^{(q)}) = \gamma(\mathbf{z})$ no matter if (3d) is enforced or not; and
- (ii) with (3d) enforced, we further have $\hat{\mathbf{c}}^{(q)} = \hat{\mathbf{f}}_P^{(q)}(\mathbf{x}^{(q)}) = \delta^{(q)}(\mathbf{c}^{(q)})$,

where $\gamma(\cdot) : \mathbb{R}^D \rightarrow \mathbb{R}^D$ and $\delta^{(q)}(\cdot) : \mathbb{R}^{D_q} \rightarrow \mathbb{R}^{D_q}$ are certain invertible functions.

Theorem 1 (i) may serve as the theoretical support to back the neural network architectures proposed in various DCCA and AM-SSL schemes, which all advocate latent correlation maximization as part of their objectives. A remark is that $\hat{\mathbf{z}} = \gamma(\mathbf{z})$ has all the information of \mathbf{z} due to the invertibility of $\gamma(\cdot)$. In addition, Theorem 1 (ii) indicates that by solving Problem (3), one can disentangle the shared and private components up to invertible nonlinear transformations.

Theorem 1 is based on the so-called *population case* (with $N = \infty$ and the \mathcal{X}_q observed). This is similar to the vast majority of provable nICA/disentanglement literature; see [2, 28–30]. Theorem 1 also relies on searching through all possible continuous functions $\mathbf{f}^{(q)}$, which may not be practical. It is of interest to study the finite sample case. In addition, considering $\mathbf{f}^{(q)} \in \mathcal{F}$, where \mathcal{F} is a certain restricted function class that may have mismatches with $\mathbf{g}^{(q)}$'s function class, is meaningful. To proceed, we assume $D_1 = D_2$ and $M = M_1 = M_2$ for notation simplicity. In addition, we have

Assumption 2 Consider the following conditions:

- (a) We have $\mathbf{f}^{(q)} \in \mathcal{F}$ and $\mathbf{g}^{(q)} \in \mathcal{G}$, respectively, where the function classes \mathcal{F} and \mathcal{G} are third-order differentiable and bounded.
- (b) The Rademacher complexity [31] of $\mathcal{F}_d = \{\mathbf{f}_d : \mathbb{R}^M \rightarrow \mathbb{R} \mid \mathbf{f}_d(\mathbf{x}) = [\mathbf{f}(\mathbf{x})]_d, \mathbf{f} \in \mathcal{F}\}$ is bounded by \mathfrak{R}_N given N samples.
- (c) Define $\mathcal{G}^{-1} = \{\mathbf{u} : \mathbb{R}^M \rightarrow \mathbb{R}^{D+D_1} \mid \mathbf{u}_S(\mathbf{x}) = \gamma(\mathbf{z}), \text{ with } \mathbf{u}_S(\mathbf{x}) = [\mathbf{u}(\mathbf{x})]_{1:D}\} \forall \mathbf{x} \in \mathcal{X}_q$ and a certain invertible γ . There exists $\mathbf{f} \in \mathcal{F}$ such that $\sup_{\mathbf{x} \in \mathcal{X}_q} \|\mathbf{f}_S(\mathbf{x}) - \mathbf{u}_S(\mathbf{x})\|_2 \leq \nu$.
- (d) For $q = 1, 2$, the elements of the third-order derivative of $\mathbf{h}^{(q)}(\mathbf{x}) = \mathbf{f}^{(q)} \circ \mathbf{g}^{(q)}(\mathbf{x})$ reside in $[-C_d, C_d]$ for all $\mathbf{x} \in \mathcal{X}_q$. In addition, $[\mathbf{c}^{(q)}]_j \in [-C_p, C_p]$ with $0 < C_p < \infty$ for $j \in [D_q]$.

Using the above assumption, we show that:

Theorem 2 Under the generative model in (2) and Assumptions 1 and 2, assume that $(\mathbf{x}_\ell^{(1)}, \mathbf{x}_\ell^{(2)})$ for $\ell = 1, \dots, N$ are i.i.d. samples of $(\mathbf{x}^{(1)}, \mathbf{x}^{(2)})$. Denote $\hat{\mathbf{f}}^{(q)} \in \mathcal{F}$ as any solution of (3) with the invertibility constraint satisfied. Then, we have the following holds with probability of at least $1 - \delta$:

$$\mathbb{E} \left[\sum_{i=1}^D \sum_{j=1}^{D_q} (\partial[\hat{\mathbf{f}}_S(\mathbf{x}^{(q)})]_i / \partial c_j^{(q)})^2 \right] = O \left(\left(D\mathfrak{R}_N + \sqrt{\log(1/\delta)/N} + \nu^2 \right)^{2/3} \right) \quad (5)$$

for any $\mathbf{c}^{(q)} \in \mathcal{C}_q$ such that $-C_p + \kappa_j \leq c_j^{(q)} \leq C_p - \kappa_j$ for all $j \in [D_q]$ and all $i \in [D]$, where $\kappa_j = \Omega((3/C_d)^{1/3} (4C_f(2D\mathfrak{R}_N + C_f\sqrt{\log(1/\delta)/2N}) + 4\nu^2)^{1/6})$.

The metric on the left hand side of (5) measures whether or not $\hat{\mathbf{f}}_S(\mathbf{x}^{(q)})$ is a function of $\mathbf{c}^{(q)}$. If this metric is zero, then $\hat{\mathbf{f}}_S(\mathbf{x}^{(q)})$ is disentangled from $\mathbf{c}^{(q)}$. The theorem indicates that with finite samples of size N , the metric is bounded by $O(N^{-1/3})$. In addition, \mathfrak{R}_N decreases when N increases; e.g., a fully connected neural network with bounded weights satisfies $\mathfrak{R}_N = O(N^{-1/2})$ [31].

The proofs of the theorems can be found in the supplementary material.

4 Implementation: Independence-Promoted Correlation Maximization

In this section, we propose an optimization strategy to realize the criterion in (3).

Enforcing Statistical Independence. A notable challenge is the statistical independence constraint in (3d), whose enforcement is often an art. Early methods such as [32, 33] are either costly or not general enough. Notably, the HSIC method in [34] that maximizes the correlation of two variables in a kernel space can be used in our framework, but kernels often induce large memory overheads and are sensitive to parameter (e.g., kernel width) selection.

Our idea for a new independence regularizer begins with the following fact. If two variables X and Y are statistically independent, then we have $p(X, Y) = p(X)p(Y) \iff \mathbb{E}[\phi(X)\tau(Y)] = \mathbb{E}[\phi(X)]\mathbb{E}[\tau(Y)]$ for all measurable functions $\phi(\cdot) : \mathbb{R} \rightarrow \mathbb{R}$ and $\tau(\cdot) : \mathbb{R} \rightarrow \mathbb{R}$ [35]. Hence, to enforce *group* independence between variables $\hat{\mathbf{z}}^{(q)}$ and $\hat{\mathbf{c}}^{(q)}$, we propose to exhaust the space of all measurable functions $\phi^{(q)} : \mathbb{R}^D \rightarrow \mathbb{R}$ and $\tau^{(q)} : \mathbb{R}^{D_q} \rightarrow \mathbb{R}$, such that

$$\sup_{\phi^{(q)}, \tau^{(q)}} \mathcal{R}^{(q)} = \sup_{\phi^{(q)}, \tau^{(q)}} |\text{Cov}[\phi^{(q)}(\hat{\mathbf{z}}^{(q)})\tau^{(q)}(\hat{\mathbf{c}}^{(q)})]| / \left(\sqrt{\mathbb{V}[\phi^{(q)}(\hat{\mathbf{z}}^{(q)})]} \sqrt{\mathbb{V}[\tau^{(q)}(\hat{\mathbf{c}}^{(q)})]} \right) \quad (6)$$

is minimized. It is not hard to show the following (see the proof in the supplementary material):

Proposition 1 In (6), if $\sup_{\phi^{(q)}, \tau^{(q)}} \mathcal{R}^{(q)} = 0$ over all measurable functions $\phi^{(q)}$ and $\tau^{(q)}$, then, any $[z]_i$ and $[c^{(q)}]_j$ for $i \in [D]$ and $j \in [D_q]$ are statistically independent.

In practice, we use two neural networks to represent $\phi^{(q)}$ and $\tau^{(q)}$, respectively, which blends well with the neural encoders for algorithm design.

Reformulation and Optimization. We use deep neural networks to serve as $f^{(q)}$. However, under this parameterization, the original criterion in (3) has neural networks in the constraints, thereby being challenging in terms of numerical optimization. To circumvent this, we introduce a slack variable \mathbf{u}_ℓ and change the objective to minimizing $\mathcal{L}_\ell = \sum_{q=1}^2 \|\mathbf{u}_\ell - \mathbf{f}_S^{(q)}(\mathbf{x}_\ell^{(q)})\|_2^2$ —which is a common trick used in neural network based multiview matching (see [21, 27]) and is reminiscent of the MAX-VAR formulation of CCA [23, 36, 37]. The slack variable can also make orthogonality and zero-mean constraints easier to enforce.

Note that attention has to be paid to the invertibility constraint in (3b). This can be enforced by using the idea of autoencoder. Namely, the reconstruction loss $\mathcal{V}_\ell = \sum_{q=1}^2 \|\mathbf{x}_\ell^{(q)} - \mathbf{r}^{(q)}(\mathbf{f}^{(q)}(\mathbf{x}_\ell^{(q)}))\|_2^2$ is employed to promote invertibility of $\mathbf{f}^{(q)}$, where $\mathbf{r}^{(q)}$ is a reconstruction network. Let $\boldsymbol{\theta}$ collect the parameters of $\mathbf{f}^{(q)}$ and $\mathbf{r}^{(q)}$, and $\boldsymbol{\eta}$ the parameters of $\phi^{(q)}, \tau^{(q)}$. The overall formulation is as follows

$$\min_{\mathbf{U}, \boldsymbol{\theta}} \max_{\boldsymbol{\eta}} \mathcal{L} + \beta \mathcal{V} + \lambda \mathcal{R}, \quad \text{s.t.} \quad \frac{1}{N} \sum_{\ell=1}^N \mathbf{u}_\ell \mathbf{u}_\ell^\top = \mathbf{I}, \quad \frac{1}{N} \sum_{\ell=1}^N \mathbf{u}_\ell = \mathbf{0}, \quad (7)$$

where $\mathcal{L} = 1/N \sum_{\ell=1}^N \mathcal{L}_\ell$, $\mathcal{V} = 1/N \sum_{\ell=1}^N \mathcal{V}_\ell$, $\mathbf{U} = [\mathbf{u}_1, \dots, \mathbf{u}_N] \in \mathbb{R}^{D \times N}$, $\mathcal{R} = \sum_{q=1}^2 \mathcal{R}^{(q)}$, and β and λ are nonnegative. In practice, $\mathbb{C}_{\text{ov}}[\cdot]$ and $\mathbb{V}[\cdot]$ are replaced using their sample, respectively. We propose a stochastic block coordinate descent algorithm for (7); see the supplementary material.

The conception of our implementation is summarized in the architecture in Fig. 1 (right).

5 Related Work - Nonlinear ICA and Latent Disentanglement

Other than the DCCA and AM-SSL works, our design for private and shared information separation also draws insights from two topics in unsupervised representation learning, namely, nICA [2, 28, 30, 38] and latent factor disentanglement [34, 39–42], which are recently offered a unifying perspective in [30]. The nICA works aim to *separate* nonlinearly mixed latent components to an individual component level, which is in general impossible unless additional information associated with each sample (e.g., time frame labels [28] and class labels [2, 30]) is used. Multiple views are less studied in the context of nICA, with the recent exception in [29]. Nonetheless, their model is different from ours and the approach cannot extract the private information using two views. None of these works offered finite sample analysis as we did in Theorem 2, to our best knowledge. Our independence promoter is reminiscent of [35], with the extension to handle group variables.

6 Experiments

All the experiments are implemented in Python (with Pytorch and TensorFlow) on a Linux workstation with 8 cores at 3.7GHz, 32GB RAM and GeForce GTX 1080 Ti GPU.

Synthetic Experiment. We construct two views as follows: The shared $\mathbf{z} \in \mathbb{R}^2$ is uniformly drawn from the unit circle, with noise $\mathcal{N}(0, 0.02^2)$ added to each dimension. We have one-dimensional $c^{(1)} \sim \mathcal{N}(0, 2.0)$ and $c^{(2)} \sim \text{Laplace}(0, 4.0)$. The shared-to-private energy ratios for the two views are approximately -6 dB and -18 dB, respectively—the interference overwhelms the “signal”. We set $N = 5,000$, and use two different one-hidden-layer neural networks with 3 neurons, softplus activation, and standard normal weights to represent the invertible $g^{(q)}$ ’s. The $\mathbf{f}^{(q)}$ is a three-hidden-layer multi-layer perceptrons (MLP) with 256 neurons in each layer with ReLU activations, and $\phi^{(q)}$ and $\tau^{(q)}$ are represented by two-hidden-layer MLPs with 128 neurons in each layer.

Table 1: Mutual information (MI) between groups of variables. “ \uparrow ”: high score preferred; “ \downarrow ”: low score preferred; “n/a”: not applicable; $\hat{z}^{(q)} = \hat{f}_S^{(q)}$ for $q = 1, 2$.

	$\hat{z}^{(1)}, z$ (\uparrow)	$\hat{z}^{(2)}, z$ (\uparrow)	$\hat{z}^{(1)}, c^{(1)}$ (\downarrow)	$\hat{z}^{(2)}, c^{(2)}$ (\downarrow)	$\hat{c}^{(1)}, c^{(1)}$ (\uparrow)	$\hat{c}^{(2)}, c^{(2)}$ (\uparrow)	$\hat{c}^{(1)}, z$ (\downarrow)	$\hat{c}^{(2)}, z$ (\downarrow)
Metric	MINE-based MI Estimation [43]							
\mathcal{L}	2.32	2.36	0.01	0.00	0.45	0.33	0.39	0.43
$\mathcal{L} + \mathcal{V}$	2.37	2.38	0.01	0.01	0.55	0.33	0.31	0.43
$\mathcal{L} + \mathcal{R}$	2.32	2.33	0.02	0.00	0.90	0.22	0.09	0.22
$\mathcal{L} + \mathcal{V} + \mathcal{R}$	2.43	2.39	0.01	0.01	1.22	0.85	0.04	0.11
$\mathcal{L} + \mathcal{V} + \text{HSIC}$	2.48	2.43	0.01	0.01	0.68	0.52	0.04	0.07
BT-Loss	0.49	0.47	0.00	0.00	n/a	n/a	n/a	n/a

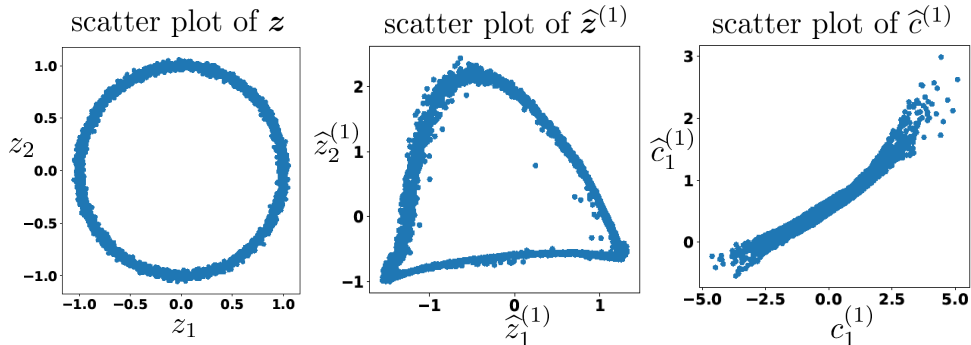


Figure 2: Visualization of synthetic data experiment; left: z ; middle: $\hat{z}^{(1)}$; right: $\hat{c}^{(1)}$.

We test the methods with different combinations of \mathcal{L} , \mathcal{R} and \mathcal{V} for ablation study purposes. We also test the performance with HSIC [34] as the independence regularizer ($\mathcal{L} + \mathcal{V} + \text{HSIC}$). In addition, we employ a baseline that uses the objective function of Barlow Twins [19] (BT-Loss).

Table 1 shows the estimated mutual information (MI) between groups of random variables of interest (measured by the mutual information neural estimation (MINE) [43]). The results are averaged from 10 random trials. One can see that all methods but the BT-Loss successfully extract the information about z in the sense that both $\hat{z}^{(q)} = \hat{f}_S^{(q)}$ for $q = 1, 2$ have similarly high MIs with z . Besides, all methods output $\hat{z}^{(q)}$ and $\hat{c}^{(q)}$ ($c^{(q)}$) that have small MIs—meaning that they are not dependent.

Although most loss functions using latent correlation maximization extract the shared z ’s information well, the difference is articulated in extracting the private information. The proposed $\mathcal{L} + \mathcal{V} + \mathcal{R}$ objective has the best performance on that regard. The method $\mathcal{L} + \mathcal{V} + \text{HSIC}$ also works reasonably well since HSIC serves the same purpose as \mathcal{R} does—but with a kernel-based implementation. Moreover, by looking at the last two columns, one can see that the methods with \mathcal{R} and \mathcal{V} perform the best in removing the information of z from $c^{(q)}$. This corroborates our analysis that both (3b) (invertibility) and (3d) (independence) are vital to achieve private-shared information disentanglement.

Fig. 2 shows $z_\ell \in \mathbb{R}^2$ and $\hat{z}_\ell^{(1)} = \hat{f}_S^{(1)}(x_\ell^{(1)})$ and $\hat{c}_\ell^{(1)} = \hat{f}_P^{(1)}(x_\ell^{(1)})$ for all ℓ . From the left and middle figures, one can clearly see that $\hat{z}_\ell^{(1)} \approx \gamma(z_\ell)$ via an invertible function γ . The right figure also shows that $\hat{c}_\ell^{(1)} \approx \delta^{(1)}(c_\ell^{(1)})$ with an invertible $\delta^{(1)}$. These results are consistent with our analysis in Theorem 1. Similar results of view 2 can be seen in the supplementary material.

Real Data: Extracting Private Latent Factors. In this section, we use the Cars3D dataset [44] that is widely employed in latent factor disentanglement experiments; see, e.g., [29, 45]. This dataset contains different car CAD models. For each car image, there are three defining aspects (namely, ‘type’, ‘elevation’ and ‘azimuth’).

We create two views as follows. We assume that given the car type that is captured by shared variables z and the azimuths that are captured by $c^{(q)}$, the generation mappings $g^{(1)}$ and $g^{(2)}$ produce car images with

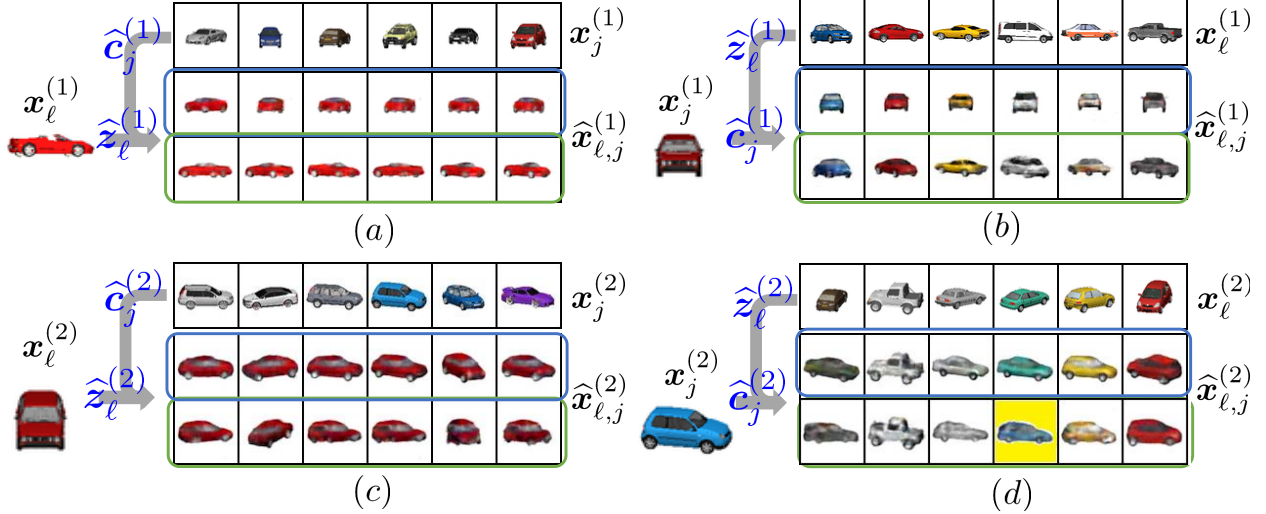


Figure 3: Evaluation on Car3D; rows in blue boxes are w/ \mathcal{R} ; rows in green boxes are w/o \mathcal{R} .

low elevations and high elevations, respectively (so they must be different mappings). Under our setting, each view has $N = 8,784$ car images. We model z with $D = 10$. For $c^{(q)}$, we set $D_1 = D_2 = 2$. More details about our settings are in the supplementary material.

We evaluate the learned $\hat{f}^{(q)}$'s by combining $\hat{z}_\ell^{(q)} = \hat{f}_S^{(q)}(x_\ell^{(q)})$ and $\hat{c}_j^{(q)} = \hat{f}_P^{(q)}(x_j^{(q)})$ and generating $\hat{x}_{\ell,j}^{(q)} = \hat{r}^{(q)}([\hat{z}_\ell^{(q)\top}, (\hat{c}_j^{(q)})^\top]^\top)$, where $\hat{r}^{(q)}$ is the learned reconstruction network [cf Eq. (7)]. Under our model, this generated sample should exhibit the same ‘type’ and ‘elevation’ as those of $x_\ell^{(q)}$ and the ‘azimuth’ of $x_j^{(q)}$. Fig. 3 shows our experiment results. The proposed method’s outputs are intuitive and desired. For example, in subfigure (a), the $z_\ell^{(1)}$ is extracted from the red convertible, and the $c_j^{(1)}$'s are extracted from the top row. One can see that the generated $\hat{x}_{\ell,j}^{(1)}$'s under the proposed method with \mathcal{R} are all red convertibles with the same elevation, but using the azimuths of the corresponding cars from the top row. Note that if \mathcal{R} is not used, then the learned $\hat{c}_j^{(q)}$ may still contain the ‘type’ or ‘elevation’ information; see the example highlighted with yellow background in subfigure (d). More results are in the supplementary material.

Real Data: AM-SSL for Image Representations. We use artificially produced views of the MNIST dataset, where one view contains randomly rotated digits and the other with additive Gaussian white noise [16]; see Fig. 4. This is similar to the data augmentation ideas in AM-SSL. The goal is to match the two views and learn the shared representations. The dataset has 70,000 samples that are 28×28 images of handwritten digits. We apply the proposed method and the benchmarking algorithms to the artificial views. We set $D = 10$, $D_1 = 20$ and $D_2 = 50$. The detailed settings of our neural networks can be found in the supplementary material.

To evaluate the effectiveness of shared information extraction, we apply k -means to all the embeddings $\hat{z}_\ell^{(1)} = \hat{f}_S^{(1)}(x_\ell^{(1)})$ and compute the clustering accuracy on the test set. In Fig. 4 (middle), we show the t-SNE [46] visualizations of $\hat{z}_\ell^{(1)}$'s on a test set of 10,000 samples together with the clustering accuracy. All results are averaged over 5 random initializations. One can see that all methods learn informative representations that are sufficiently distinguishable, which corroborates our analysis in Theorem 1 (i)—i.e., latent correlation maximization alone suffices to extract the distortion-invariant information; see more results in the supplementary material.

To see the effectiveness of the \mathcal{R} regularization, we show the cross-view generation results in Fig. 4 (right). Here, we extract $\hat{z}_\ell^{(2)} = \hat{f}_S^{(2)}(x_\ell^{(2)})$ from the second view and $\hat{c}_j^{(1)} = \hat{f}_P^{(1)}(x_j^{(1)})$ from the first. Then,

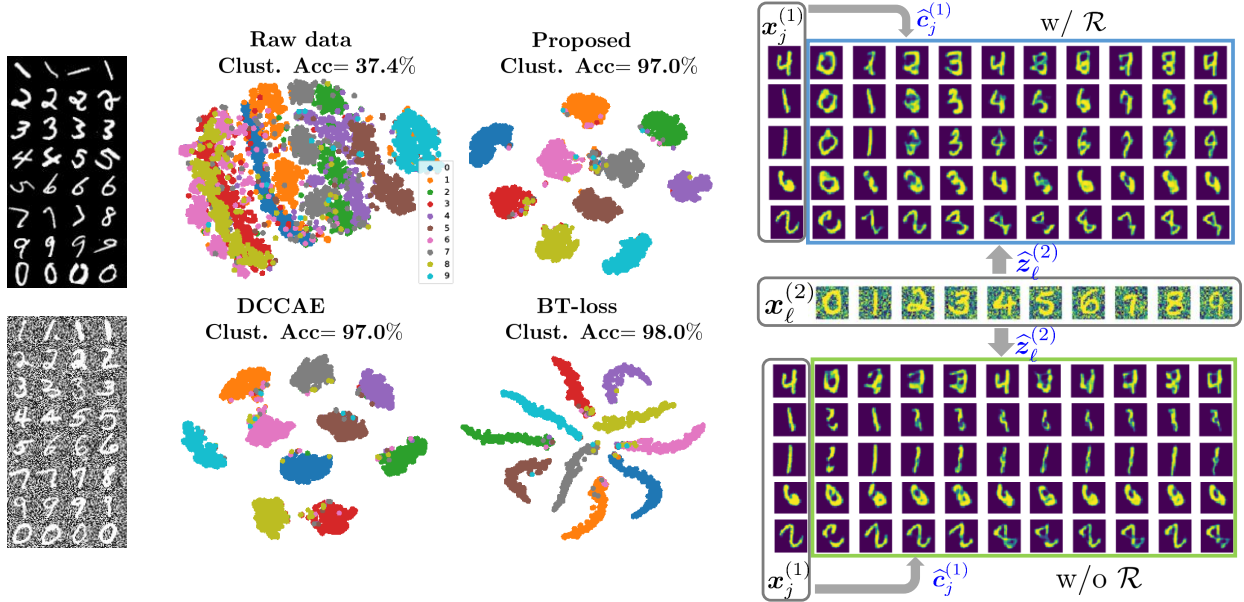


Figure 4: Left: samples of view 1 (top) and view 2 (bottom); middle: t-SNE of the raw data and learned representations; right: cross-view generation from $x_\ell^{(2)}$ to $x_\ell^{(1)}$.

we generate $\hat{x}_{\ell,j}^{(1)} = \hat{r}^{(1)}([\hat{z}_\ell^{(2)\top}, (\mathbf{c}_j^{(1)})^\top]^\top)$ shown in the blue and green boxes. Ideally, the generated samples should have the class information of $x_\ell^{(2)}$ (contained in $\hat{z}_\ell^{(2)}$) while the style information of $x_j^{(1)}$ (contained in $\hat{c}_j^{(1)}$). Clearly, using \mathcal{R} attains the desired results. Note that this dataset is challenging as the noise in view 2 is very high, making it hard to achieve perfect matching and reconstruction—but our result is still plausible; see more details in the supplementary material.

7 Conclusion

We proposed a multiview representation learning framework with provable guarantees. In particular, we modeled multiview data as nonlinear mixtures of shared and private components, and provided a learning framework that ensures to disentangle the shared and private information, under reasonable conditions. We also analyzed the sample complexity for extracting the shared information, which is the first of its kind, to our best knowledge. To realize our learning criterion, we proposed a slack variable-assisted latent correlation maximization approach, with a novel minimax neural regularizer for promoting group independence. We tested our method over synthetic and real data, and the results corroborated our design goals and theoretical analyses.

Limitations and Future Work. First, some assumptions are not always mild, e.g., exact identical shared information and known latent dimensions. In addition, invertibility of the generative process is not easy to check or guarantee, which may affect applicability. Last, despite its practical effectiveness, convergence theory of the algorithm is elusive, since a hard-to-analyze minimax problem is involved. These aspects could be further studied in the future.

References

- [1] G. E. Hinton and R. S. Zemel, "Autoencoders, minimum description length and Helmholtz free energy," in *Advances in Neural Information Processing Systems*, 1994, pp. 3–10.
- [2] A. Hyvarinen, H. Sasaki, and R. Turner, "Nonlinear ICA using auxiliary variables and generalized contrastive learning," in *International Conference on Artificial Intelligence and Statistics*, 2019, pp. 859–868.
- [3] Y. Tian, D. Krishnan, and P. Isola, "Contrastive multiview coding," *arXiv preprint arXiv:1906.05849*, 2019.
- [4] T. Chen, S. Kornblith, M. Norouzi, and G. Hinton, "A simple framework for contrastive learning of visual representations," in *International Conference on Machine Learning*. PMLR, 2020, pp. 1597–1607.
- [5] A. Dosovitskiy, P. Fischer, J. T. Springenberg, M. Riedmiller, and T. Brox, "Discriminative unsupervised feature learning with exemplar convolutional neural networks," *IEEE Trans. Pattern Anal. Mach. Intell.*, vol. 38, no. 9, pp. 1734–1747, 2015.
- [6] S. Gidaris, P. Singh, and N. Komodakis, "Unsupervised representation learning by predicting image rotations," in *International Conference on Learning Representations*, 2018.
- [7] C. Doersch, A. Gupta, and A. A. Efros, "Unsupervised visual representation learning by context prediction," in *Proceedings of the IEEE International Conference on Computer Vision*, 2015, pp. 1422–1430.
- [8] D. Pathak, P. Krahenbuhl, J. Donahue, T. Darrell, and A. A. Efros, "Context encoders: Feature learning by inpainting," in *Proceedings of the IEEE Conference on Computer Vision and Pattern Recognition*, 2016, pp. 2536–2544.
- [9] H. Hotelling, "Relations between two sets of variates," *Biometrika*, vol. 28, no. 3/4, pp. 321–377, 1936.
- [10] T. G. Kolda and B. W. Bader, "Tensor decompositions and applications," *SIAM Review*, vol. 51, no. 3, pp. 455–500, 2009.
- [11] P. Geladi and B. R. Kowalski, "Partial least-squares regression: A tutorial," *Analytica chimica acta*, vol. 185, pp. 1–17, 1986.
- [12] F. R. Bach and M. I. Jordan, "A probabilistic interpretation of canonical correlation analysis," 2005.
- [13] M. S. Ibrahim and N. D. Sidiropoulos, "Reliable detection of unknown cell-edge users via canonical correlation analysis," *IEEE Trans. Wireless Commun.*, vol. 19, no. 6, pp. 4170–4182, 2020.
- [14] P. L. Lai and C. Fyfe, "Kernel and nonlinear canonical correlation analysis," *International Journal of Neural Systems*, vol. 10, no. 05, pp. 365–377, 2000.
- [15] G. Andrew, R. Arora, J. Bilmes, and K. Livescu, "Deep canonical correlation analysis," in *International Conference on Machine Learning*. PMLR, 2013, pp. 1247–1255.
- [16] W. Wang, R. Arora, K. Livescu, and J. Bilmes, "On deep multi-view representation learning," in *International Conference on Machine Learning*, 2015, pp. 1083–1092.
- [17] J.-B. Grill, F. Strub, F. Altché, C. Tallec, P. Richemond, E. Buchatskaya, C. Doersch, B. Avila Pires, Z. Guo, M. Gheshlaghi Azar, B. Piot, k. kavukcuoglu, R. Munos, and M. Valko, "Bootstrap your own latent - a new approach to self-supervised learning," in *Advances in Neural Information Processing Systems*, vol. 33, 2020, pp. 21 271–21 284.
- [18] X. Chen and K. He, "Exploring simple Siamese representation learning," *arXiv preprint arXiv:2011.10566*, 2020.

- [19] J. Zbontar, L. Jing, I. Misra, Y. LeCun, and S. Deny, “Barlow Twins: Self-supervised learning via redundancy reduction,” *arXiv preprint arXiv:2103.03230*, 2021.
- [20] W. Wang, R. Arora, K. Livescu, and J. A. Bilmes, “Unsupervised learning of acoustic features via deep canonical correlation analysis,” in *IEEE International Conference on Acoustics, Speech and Signal Processing (ICASSP)*, 2015, pp. 4590–4594.
- [21] A. Benton, H. Khayrallah, B. Gujral, D. Reisinger, S. Zhang, and R. Arora, “Deep generalized canonical correlation analysis,” in *RepL4NLP at ACL*, 2017.
- [22] A. Gretton, O. Bousquet, A. Smola, and B. Schölkopf, “Measuring statistical dependence with hilbertschmidt norms,” in *International Conference on Algorithmic Learning Theory*. Springer, 2005, pp. 63–77.
- [23] J. D. Carroll, “Generalization of canonical correlation analysis to three or more sets of variables,” in *Proceedings of the 76th annual convention of the American Psychological Association*, vol. 3, 1968, pp. 227–228.
- [24] X. Huang, M.-Y. Liu, S. Belongie, and J. Kautz, “Multimodal unsupervised image-to-image translation,” in *Proceedings of the European Conference on Computer Vision*, 2018, pp. 172–189.
- [25] H.-Y. Lee, H.-Y. Tseng, J.-B. Huang, M. Singh, and M.-H. Yang, “Diverse image-to-image translation via disentangled representations,” in *Proceedings of the European Conference on Computer Vision*, 2018, pp. 35–51.
- [26] A. Hyvärinen and P. Pajunen, “Nonlinear Independent Component Analysis: Existence and uniqueness results,” *Neural Networks*, vol. 12, no. 3, pp. 429–439, 1999.
- [27] Q. Lyu and X. Fu, “Nonlinear multiview analysis: Identifiability and neural network-assisted implementation,” *IEEE Trans. Signal Process.*, vol. 68, pp. 2697–2712, 2020.
- [28] A. Hyvarinen and H. Morioka, “Unsupervised feature extraction by time-contrastive learning and nonlinear ica,” in *Advances in Neural Information Processing Systems*, vol. 29, 2016.
- [29] F. Locatello, B. Poole, G. Rätsch, B. Schölkopf, O. Bachem, and M. Tschannen, “Weakly-supervised disentanglement without compromises,” in *International Conference on Machine Learning*. PMLR, 2020, pp. 6348–6359.
- [30] I. Khemakhem, D. Kingma, R. Monti, and A. Hyvarinen, “Variational autoencoders and nonlinear ICA: A unifying framework,” in *International Conference on Artificial Intelligence and Statistics*. PMLR, 2020, pp. 2207–2217.
- [31] S. Shalev-Shwartz and S. Ben-David, *Understanding machine learning: From theory to algorithms*. Cambridge university press, 2014.
- [32] A. Taleb and C. Jutten, “Source separation in post-nonlinear mixtures,” *IEEE Trans. Signal Process.*, vol. 47, no. 10, pp. 2807–2820, 1999.
- [33] A. Hyvärinen and E. Oja, “Independent component analysis: Algorithms and applications,” *Neural Networks*, vol. 13, no. 4-5, pp. 411–430, 2000.
- [34] R. Lopez, J. Regier, M. I. Jordan, and N. Yosef, “Information constraints on auto-encoding variational Bayes,” *Advances in Neural Information Processing Systems*, vol. 31, pp. 6114–6125, 2018.
- [35] A. Gretton, A. J. Smola, O. Bousquet, R. Herbrich, A. Belitski, M. Augath, Y. Murayama, J. Pauls, B. Schölkopf, and N. K. Logothetis, “Kernel constrained covariance for dependence measurement.” in *International Conference on Artificial Intelligence and Statistics*, vol. 10. Citeseer, 2005, pp. 112–119.
- [36] J. R. Kettenring, “Canonical analysis of several sets of variables,” *Biometrika*, vol. 58, no. 3, pp. 433–451, 1971.

- [37] P. Rastogi, B. Van Durme, and R. Arora, "Multiview LSA: Representation learning via generalized CCA," in *Proceedings of the 2015 conference of the North American chapter of the Association for Computational Linguistics: Human Language Technologies*, 2015, pp. 556–566.
- [38] A. Hyvarinen and H. Morioka, "Nonlinear ICA of temporally dependent stationary sources," in *International Conference on Artificial Intelligence and Statistics*, vol. 54, 20–22 Apr 2017, pp. 460–469.
- [39] I. Higgins, L. Matthey, A. Pal, C. Burgess, X. Glorot, M. Botvinick, S. Mohamed, and A. Lerchner, "Beta-VAE: Learning basic visual concepts with a constrained variational framework," in *International Conference on Learning Representations*, 2017.
- [40] H. Kim and A. Mnih, "Disentangling by factorising," in *International Conference on Machine Learning*, vol. 80. PMLR, 10–15 Jul 2018, pp. 2649–2658.
- [41] R. T. Chen, X. Li, R. B. Grosse, and D. K. Duvenaud, "Isolating sources of disentanglement in variational autoencoders," in *Advances in Neural Information Processing Systems*, 2018, pp. 2610–2620.
- [42] S. Zhao, J. Song, and S. Ermon, "InfoVAE: Balancing learning and inference in variational autoencoders," *Proceedings of the AAAI Conference on Artificial Intelligence*, vol. 33, no. 01, pp. 5885–5892, Jul. 2019.
- [43] M. I. Belghazi, A. Baratin, S. Rajeshwar, S. Ozair, Y. Bengio, A. Courville, and D. Hjelm, "MINE: Mutual information neural estimation," in *International Conference on Machine Learning*, vol. 80. PMLR, 10–15 Jul 2018, pp. 531–540.
- [44] S. E. Reed, Y. Zhang, Y. Zhang, and H. Lee, "Deep visual analogy-making," *Advances in Neural Information Processing Systems*, vol. 28, pp. 1252–1260, 2015.
- [45] F. Locatello, S. Bauer, M. Lucic, G. Raetsch, S. Gelly, B. Schölkopf, and O. Bachem, "Challenging common assumptions in the unsupervised learning of disentangled representations," in *International Conference on Machine Learning*. PMLR, 2019, pp. 4114–4124.
- [46] G. Hinton and S. T. Roweis, "Stochastic neighbor embedding," in *Advances in Neural Information Processing Systems*, vol. 15, 2002, pp. 833–840.
- [47] L. Gresele, P. K. Rubenstein, A. Mehrjou, F. Locatello, and B. Schölkopf, "The incomplete Rosetta stone problem: Identifiability results for multi-view nonlinear ICA," in *Proceedings of UAI 2020*, 2020, pp. 217–227.
- [48] P. L. Bartlett and S. Mendelson, "Rademacher and Gaussian complexities: Risk bounds and structural results," *Journal of Machine Learning Research*, vol. 3, no. Nov, pp. 463–482, 2002.
- [49] M. Mohri, A. Rostamizadeh, and A. Talwalkar, *Foundations of Machine Learning*. MIT press, 2018.
- [50] R. A. Fisher, "Frequency distribution of the values of the correlation coefficient in samples from an indefinitely large population," *Biometrika*, vol. 10, no. 4, pp. 507–521, 1915.
- [51] D. P. Kingma and J. Ba, "Adam: A method for stochastic optimization," *arXiv preprint arXiv:1412.6980*, 2014.
- [52] J. Duchi, E. Hazan, and Y. Singer, "Adaptive subgradient methods for online learning and stochastic optimization," *Journal of Machine Learning Research*, vol. 12, no. Jul, pp. 2121–2159, 2011.
- [53] R. A. Davis, K.-S. Lii, and D. N. Politis, "Remarks on some nonparametric estimates of a density function," in *Selected Works of Murray Rosenblatt*. Springer, 2011, pp. 95–100.
- [54] K. Y. Yeung and W. L. Ruzzo, "Details of the Adjusted Rand Index and clustering algorithms, supplement to the paper an empirical study on Principal Component Analysis for clustering gene expression data," *Bioinformatics*, vol. 17, no. 9, pp. 763–774, 2001.

Supplementary Materials for “Latent Correlation-Based Multiview Learning and Self-Supervision: A Unifying Perspective”

A Notation

The notations used in this work are summarized in Table A.1.

Notation	Definition
$x, \mathbf{x}, \mathbf{X}$	scalar, vector, and matrix
$[\mathbf{x}]_i, x_i$	both represent the i th element of vector \mathbf{x}
$[\mathbf{X}]_{ij}$	the i th row, j th column of matrix \mathbf{X}
$p(\mathbf{x})$	probability density function of random variable \mathbf{x}
$x \perp\!\!\!\perp y$	x and y are statistically independent, i.e., $p(x, y) = p(x)p(y)$
$\mathbf{x} \perp\!\!\!\perp \mathbf{y}$	$x_i \perp\!\!\!\perp y_j$ for all i, j
$\mathbf{x}^\top, \mathbf{X}^\top$	transpose of \mathbf{x}, \mathbf{X}
\mathbf{J}_f	Jacobian matrix of a vector-valued function f
\mathbf{I}	identity matrix with a proper size
$f \circ g$	function composition operation
$\det \mathbf{X}$	determinant of a square matrix \mathbf{X}
$\mathbb{E}[\cdot]$	expectation
$\mathbb{V}[\cdot]$	variance
$\text{Cov}[\cdot, \cdot]$	covariance
$[N]$	the integer set $\{1, 2, \dots, N\}$

B Proof of Theorem 1

Theorem 1. Under the generative model in (2) and Assumption 1, and assume that $p(\mathbf{z}) > 0$ and $p(\mathbf{c}^{(q)}) > 0$ for all $\mathbf{z} \in \mathcal{Z}$, $\mathbf{c}^{(q)} \in \mathcal{C}_q$. Consider the population form in (3) (i.e., $N = \infty$). Assume that the considered constraints hold over all $\mathbf{x}^{(q)} \in \mathcal{X}_q$ for $q = 1, 2$, where $\mathcal{X}_q = \{\mathbf{x}^{(q)} | \mathbf{x}^{(q)} = \mathbf{g}^{(q)}([\mathbf{z}^\top, (\mathbf{c}^{(q)})^\top]^\top), \forall \mathbf{z} \in \mathcal{Z}, \forall \mathbf{c}^{(q)} \in \mathcal{C}_q\}$. Denote $\hat{\mathbf{f}}^{(q)}$ as *any* solution of (3). Also assume that the first-order derivative of $\hat{\mathbf{f}}^{(q)} \circ \mathbf{g}^{(q)}$ exists. Then, we have

- (i) $\hat{\mathbf{z}} = \hat{\mathbf{f}}_S^{(q)}(\mathbf{x}^{(q)}) = \gamma(\mathbf{z})$ no matter if (3d) is enforced or not; and
- (ii) with (3d) enforced, we further have $\hat{\mathbf{c}}^{(q)} = \hat{\mathbf{f}}_P^{(q)}(\mathbf{x}^{(q)}) = \delta^{(q)}(\mathbf{c}^{(q)})$,

where $\gamma(\cdot) : \mathbb{R}^D \rightarrow \mathbb{R}^D$ and $\delta^{(q)}(\cdot) : \mathbb{R}^{D_q} \rightarrow \mathbb{R}^{D_q}$ are certain invertible functions.

We will use the following lemma:

Lemma 1 Assume that x, y are independent continuous random variables, and that $p(x) > 0$ for $x \in \mathcal{X}$ and $p(y) > 0$ for $y \in \mathcal{Y}$, where \mathcal{X} and \mathcal{Y} are open continuous sets. Treat x as a function of y , i.e., $x = x(y)$. Then, we always have

$$\frac{dx}{dy} := \lim_{\delta \rightarrow 0} \frac{x(y + \delta) - x(y)}{\delta} = 0, \forall (x, y) \in \mathcal{X} \times \mathcal{Y}. \quad (\text{B.1})$$

The same holds for dy/dx by role symmetry.

Remark 1 Taking derivative of a random variable (x) w.r.t. another random variable (y) and using $dx/dy = 0$ seems to be a well accepted trick in many nICA works; see, e.g., [32, 38, 47]. Nonetheless, we did not find a reference or derivation to support this seemingly intuitive conclusion. Hence, we derive Lemma 1 to support this already widely used trick.

Proof: We will show the lemma by contradiction. Assume there exists certain point (x_0, y_0) such that

$$\left. \frac{dx}{dy} \right|_{y=y_0} = \lim_{\delta \rightarrow 0} \frac{x(y_0 + \delta) - x(y_0)}{\delta} = \rho \neq 0. \quad (\text{B.2})$$

where $x(y_0) = x_0$. Then we have that $p(x_0 + \rho\delta, y_0 + \delta) \neq 0$ for certain $\delta > 0$. This is because $x(y_0 + \delta) = \rho\delta + x_0$ when $\rho \neq 0$, and thus the probability mass of $(\rho\delta + x_0, y_0 + \delta)$ in $\mathcal{X} \times \mathcal{Y}$ cannot be zero.

By the same reason, Eq. (B.2) also indicates that we have $p(x_0, y_0 + \delta) = 0$ since $\rho \neq 0$. However, by definition of statistical independence we have the following

$$p(x, y) = p(x)p(y) \neq 0, \quad \forall (x, y),$$

due to the assumption that

$$p(x) > 0, p(y) > 0, \quad \forall x \in \mathcal{X}, y \in \mathcal{Y}.$$

Therefore, we have reached a contradiction here. \square

B.1 The (i) Part

We first consider the formulation in (3) *without* (3d). When $N = \infty$ and $\mathbf{x}^{(q)} \sim \mathcal{X}_q$ for $q = 1, 2$ are all available, the sample average version of the formulation in (3) becomes the following expected value version:

$$\underset{\mathbf{f}^{(1)}, \mathbf{f}^{(2)}}{\text{maximize}} \text{Tr} \left(\mathbb{E} \left[\mathbf{f}_S^{(1)}(\mathbf{x}_\ell^{(1)}) \left(\mathbf{f}_S^{(2)}(\mathbf{x}_\ell^{(2)})^\top \right) \right] \right) \quad (\text{B.3a})$$

$$\text{subject to } \mathbf{f}^{(q)} \text{ for } q = 1, 2 \text{ are invertible,} \quad (\text{B.3b})$$

$$\mathbb{E} \left[\mathbf{f}_S^{(q)}(\mathbf{x}_\ell^{(q)}) \mathbf{f}_S^{(q)}(\mathbf{x}_\ell^{(q)})^\top \right] = \mathbf{I}, \quad \mathbb{E} \left[\mathbf{f}_S(\mathbf{x}_\ell^{(q)}) \right] = \mathbf{0}, \quad q = 1, 2 \quad (\text{B.3c})$$

First, note that under the generative model in (2), the maximum of the objective function in (3) is D , which is obtained when every corresponding components of the learned solutions, i.e., $\hat{\mathbf{f}}_S^{(1)} : \mathbb{R}^{M_1} \rightarrow \mathbb{R}^D$ and $\hat{\mathbf{f}}_S^{(2)} : \mathbb{R}^{M_2} \rightarrow \mathbb{R}^D$, are perfectly correlated, i.e.,

$$\hat{\mathbf{f}}_S^{(1)}(\mathbf{x}^{(1)}) = \hat{\mathbf{f}}_S^{(2)}(\mathbf{x}^{(2)}). \quad (\text{B.4})$$

Indeed, one may rewrite (B.3a) as

$$\begin{aligned} & \arg \min_{\mathbf{f}^{(1)}, \mathbf{f}^{(2)}} -2\text{Tr} \left(\mathbb{E} \left[\mathbf{f}_S^{(1)}(\mathbf{x}_\ell^{(1)}) \left(\mathbf{f}_S^{(2)}(\mathbf{x}_\ell^{(2)})^\top \right) \right] \right) \\ &= \arg \min_{\mathbf{f}^{(1)}, \mathbf{f}^{(2)}} \mathbf{I} - 2\text{Tr} \left(\mathbb{E} \left[\mathbf{f}_S^{(1)}(\mathbf{x}_\ell^{(1)}) \left(\mathbf{f}_S^{(2)}(\mathbf{x}_\ell^{(2)})^\top \right) \right] \right) + \mathbf{I} \\ &= \arg \min_{\mathbf{f}^{(1)}, \mathbf{f}^{(2)}} \mathbb{E} \left[\left\| \mathbf{f}_S^{(1)}(\mathbf{x}_\ell^{(1)}) - \mathbf{f}_S^{(2)}(\mathbf{x}_\ell^{(2)}) \right\|_2^2 \right] \end{aligned} \quad (\text{B.5})$$

where the second equality holds because the constraint in (B.3c). Note that the criterion in (B.5) admits the optimal solution in (B.4) under our generative model.

Note that one solution to attain zero cost of (B.5) is

$$\hat{\mathbf{f}}_S^{(q)}(\mathbf{x}^{(q)}) = \mathbf{z}, \quad q = 1, 2.$$

However, the question lies in “uniqueness”, i.e., can enforcing (B.4) always yield $\mathbf{f}_S^{(q)}(\mathbf{x}^{(q)}) = \mathbf{z}$ (up to certain ambiguities)? This is central to learning criterion design, as the expressiveness of function approximators like neural networks may attain zero cost of (B.5) with undesired solutions.

Assume that a solution that satisfies (B.4) is found. Denote $\widehat{\mathbf{f}}^{(q)}$ for $q = 1, 2$ as the solution. Combine the solution with the generative model in (2). Then, following equality can be obtained:

$$\mathbf{h}_S^{(1)} \left(\begin{bmatrix} \mathbf{z} \\ \mathbf{c}^{(1)} \end{bmatrix} \right) = \mathbf{h}_S^{(2)} \left(\begin{bmatrix} \mathbf{z} \\ \mathbf{c}^{(2)} \end{bmatrix} \right), \quad (\text{B.6})$$

where we have

$$\mathbf{h}_S^{(q)}(\mathbf{x}^{(q)}) = \left[\widehat{\mathbf{f}}^{(q)} \circ \mathbf{g}^{(q)}(\mathbf{x}^{(q)}) \right]_{1:D} = \widehat{\mathbf{f}}_S^{(q)} \circ \mathbf{g}^{(q)}(\mathbf{x}^{(q)}).$$

We hope to show that $\mathbf{h}_S^{(1)}$ and $\mathbf{h}_S^{(2)}$ are functions of only \mathbf{z} —i.e., the functions $\mathbf{f}_S^{(q)}$ for $q = 1, 2$ only extract the shared information.

Using the condition in (4), i.e.,

$$\mathbf{z} \perp\!\!\!\perp \mathbf{c}^{(1)}, \mathbf{z} \perp\!\!\!\perp \mathbf{c}^{(2)}, \mathbf{c}^{(1)} \perp\!\!\!\perp \mathbf{c}^{(2)},$$

the first-order derivatives satisfy the following:

$$\frac{\partial z_i}{\partial c_j^{(q)}} = 0, \quad q = 1, 2, \quad i \in [D], \quad j \in [D_q], \quad (\text{B.7})$$

$$\frac{\partial c_i^{(2)}}{\partial c_j^{(1)}} = 0, \quad i \in [D_2], \quad j \in [D_1], \quad (\text{B.8})$$

for all $\mathbf{z} \in \text{int}\mathcal{Z}$ and $\mathbf{c}^{(q)} \in \text{int}\mathcal{C}_q$, where $z_i = [\mathbf{z}]_i$ and $c_j^{(q)} = [\mathbf{c}^{(q)}]_j$ —where we have the marginal $p(z_i) > 0$ and $p(c_j^{(q)}) > 0$ due to the assumption that the joint probability $p(\mathbf{z}) > 0$ and $p(\mathbf{c}^{(1)}) > 0$ and we can use Lemma 1 to obtain (B.7) and (B.8). Let us define matrices $\mathbf{H}_S^{(1)}$ and $\mathbf{H}_S^{(2)}$, where

$$\left[\mathbf{H}_S^{(q)} \right]_{i,j} = \frac{\partial \left[\mathbf{h}_S^{(q)}(\mathbf{x}^{(q)}) \right]_i}{\partial c_j^{(1)}}, \quad i = 1, \dots, D, \quad j = 1, \dots, D_1.$$

By taking partial derivatives w.r.t. $c_j^{(1)}$ on Eq. (B.6) and putting the results together, we have

$$\mathbf{H}_S^{(1)} = \mathbf{H}_S^{(2)} \stackrel{(a)}{=} \mathbf{J}_{\mathbf{h}_S^{(2)}} \begin{bmatrix} \frac{\partial z_1}{\partial c_1^{(1)}} & \dots & \frac{\partial z_1}{\partial c_{D_1}^{(1)}} \\ \vdots & \ddots & \vdots \\ \frac{\partial z_D}{\partial c_1^{(1)}} & \dots & \frac{\partial z_D}{\partial c_{D_1}^{(1)}} \\ \frac{\partial c_1^{(2)}}{\partial c_1^{(1)}} & \dots & \frac{\partial c_1^{(2)}}{\partial c_{D_1}^{(1)}} \\ \vdots & \ddots & \vdots \\ \frac{\partial c_{D_2}^{(2)}}{\partial c_1^{(1)}} & \dots & \frac{\partial c_{D_2}^{(2)}}{\partial c_{D_1}^{(1)}} \end{bmatrix} \stackrel{(b)}{=} \mathbf{J}_{\mathbf{h}_S^{(2)}} \begin{bmatrix} \mathbf{0}_{D \times D_1} \\ \mathbf{0}_{D_2 \times D_1} \end{bmatrix} = \mathbf{0}_{D \times D_1},$$

where $\mathbf{J}_{\mathbf{h}_S^{(2)}} \in \mathbb{R}^{D \times (D+D_2)}$ is the Jacobian of $\mathbf{h}_S^{(2)}$, (a) is by the chain rules and (b) is by applying (B.7)-(B.8).

The equation above indicates that the learned $\mathbf{h}_S^{(q)}(\mathbf{x}^{(q)})$ is not a function of $\mathbf{c}^{(1)}$, since chances that $\mathbf{h}_S^{(q)}(\mathbf{x}^{(q)})$ is a constant have been eliminated by function invertibility.

Next, let us denote the outputs of $\mathbf{h}^{(1)} = \widehat{\mathbf{f}}^{(1)} \circ \mathbf{g}^{(1)}(\mathbf{x}^{(1)})$ as follows:

$$\begin{bmatrix} \widehat{\mathbf{z}} \\ \widehat{\mathbf{c}}^{(1)} \end{bmatrix} = \mathbf{h}^{(1)} \left(\begin{bmatrix} \mathbf{z} \\ \mathbf{c}^{(1)} \end{bmatrix} \right). \quad (\text{B.9})$$

The Jacobian of $\mathbf{h}^{(1)}$ can be expressed using the following block form:

$$\mathbf{J}^{(1)} = \begin{bmatrix} \mathbf{J}_{11}^{(1)} & \mathbf{H}_S^{(1)} \\ \mathbf{J}_{21}^{(1)} & \mathbf{J}_{22}^{(1)} \end{bmatrix} = \begin{bmatrix} \mathbf{J}_{11}^{(1)} & \mathbf{0}_{D \times D_1} \\ \mathbf{J}_{21}^{(1)} & \mathbf{J}_{22}^{(1)} \end{bmatrix},$$

where $\mathbf{J}_{11}^{(1)} \in \mathbb{R}^{D \times D}$, $\mathbf{J}_{21}^{(1)} \in \mathbb{R}^{D_1 \times D}$ and $\mathbf{J}_{22}^{(1)} \in \mathbb{R}^{D_1 \times D_1}$ are Jacobian matrices defined as follows

$$\mathbf{J}_{11}^{(1)} = \begin{bmatrix} \frac{\partial [\mathbf{h}_S^{(1)}(\mathbf{x}^{(1)})]_1}{\partial z_1} & \dots & \frac{\partial [\mathbf{h}_S^{(1)}(\mathbf{x}^{(1)})]_1}{\partial z_D} \\ \vdots & \ddots & \vdots \\ \frac{\partial [\mathbf{h}_S^{(1)}(\mathbf{x}^{(1)})]_D}{\partial z_1} & \dots & \frac{\partial [\mathbf{h}_S^{(1)}(\mathbf{x}^{(1)})]_D}{\partial z_D} \end{bmatrix}, \quad \mathbf{J}_{21}^{(1)} = \begin{bmatrix} \frac{\partial [\mathbf{h}_P^{(1)}(\mathbf{x}^{(1)})]_1}{\partial z_1} & \dots & \frac{\partial [\mathbf{h}_P^{(1)}(\mathbf{x}^{(1)})]_1}{\partial z_D} \\ \vdots & \ddots & \vdots \\ \frac{\partial [\mathbf{h}_P^{(1)}(\mathbf{x}^{(1)})]_{D_1}}{\partial z_1} & \dots & \frac{\partial [\mathbf{h}_P^{(1)}(\mathbf{x}^{(1)})]_{D_1}}{\partial z_D} \end{bmatrix},$$

$$\mathbf{J}_{22}^{(1)} = \begin{bmatrix} \frac{\partial [\mathbf{h}_P^{(1)}(\mathbf{x}^{(1)})]_1}{\partial c_1^{(1)}} & \dots & \frac{\partial [\mathbf{h}_P^{(1)}(\mathbf{x}^{(1)})]_1}{\partial c_{D_1}^{(1)}} \\ \vdots & \ddots & \vdots \\ \frac{\partial [\mathbf{h}_P^{(1)}(\mathbf{x}^{(1)})]_{D_1}}{\partial c_1^{(1)}} & \dots & \frac{\partial [\mathbf{h}_P^{(1)}(\mathbf{x}^{(1)})]_{D_1}}{\partial c_{D_1}^{(1)}} \end{bmatrix}.$$

By the structure of the Jacobian $\mathbf{J}^{(1)}$, one can see that $\widehat{\mathbf{z}}$ a function of only \mathbf{z} , which we denote as $\widehat{\mathbf{z}} = \gamma(\mathbf{z})$. This proves our claim (i). \square

B.2 The (ii) Part

Following the proof of Part (i), we further consider the expected value version with (3d), i.e.,

$$\underset{\mathbf{f}^{(1)}, \mathbf{f}^{(2)}}{\text{maximize}} \text{Tr} \left(\mathbb{E} \left[\mathbf{f}_S^{(1)}(\mathbf{x}^{(1)}) \mathbf{f}_S^{(2)}(\mathbf{x}^{(2)})^\top \right] \right) \quad (\text{B.10a})$$

$$\text{subject to } \mathbf{f}^{(q)} \text{ for } q = 1, 2 \text{ are invertible,} \quad (\text{B.10b})$$

$$\mathbb{E} \left[\mathbf{f}_S^{(q)}(\mathbf{x}^{(q)}) \mathbf{f}_S^{(q)}(\mathbf{x}^{(q)})^\top \right] = \mathbf{I}, \quad \mathbb{E} \left[\mathbf{f}_S^{(q)}(\mathbf{x}^{(q)}) \right] = \mathbf{0}, \quad q = 1, 2, \quad (\text{B.10c})$$

$$\mathbf{f}_S^{(q)}(\mathbf{x}^{(q)}) \perp\!\!\!\perp \mathbf{f}_P^{(q)}(\mathbf{x}^{(q)}), \quad q = 1, 2, \quad (\text{B.10d})$$

Again, under our generative model, any optimal solution $(\widehat{\mathbf{f}}^{(1)}, \widehat{\mathbf{f}}^{(2)})$ satisfies

$$\widehat{\mathbf{f}}_S^{(1)}(\mathbf{x}^{(1)}) = \widehat{\mathbf{f}}_S^{(2)}(\mathbf{x}^{(2)}).$$

We will further show that

$$\widehat{\mathbf{c}}^{(q)} = \widehat{\mathbf{f}}_P^{(q)}(\mathbf{x}^{(q)}) = \mathbf{h}_P^{(1)} \left(\begin{bmatrix} \mathbf{z} \\ \mathbf{c}^{(1)} \end{bmatrix} \right)$$

is an invertible function-transformed version of $\mathbf{c}^{(q)}$.

To further show that $\widehat{\mathbf{c}}^{(1)}$ is only a function of $\mathbf{c}^{(1)}$. First, observe that

$$\mathbf{J}_{21}^{(1)} = \begin{bmatrix} \frac{\partial [\mathbf{h}_P^{(1)}(\mathbf{x}^{(1)})]_1}{\partial \widehat{z}_1} & \dots & \frac{\partial [\mathbf{h}_P^{(1)}(\mathbf{x}^{(1)})]_1}{\partial \widehat{z}_D} \\ \vdots & \ddots & \vdots \\ \frac{\partial [\mathbf{h}_P^{(1)}(\mathbf{x}^{(1)})]_{D_1}}{\partial \widehat{z}_1} & \dots & \frac{\partial [\mathbf{h}_P^{(1)}(\mathbf{x}^{(1)})]_{D_1}}{\partial \widehat{z}_D} \end{bmatrix} \mathbf{J}_{11}^{(1)},$$

where the first matrix on the right hand side is the Jacobian of $\widehat{\mathbf{c}}^{(1)}$ w.r.t. $\widehat{\mathbf{z}}$.

By (B.10d), we have $\widehat{\mathbf{c}}^{(1)} \perp\!\!\!\perp \widehat{\mathbf{z}}$. In addition, we have $p(\widehat{z}_j) > 0$ due to $p(\widehat{\mathbf{z}}) = \frac{1}{|\det \mathbf{J}_{11}^{(1)}|} p(\mathbf{z}) > 0$; i.e., the joint distribution $p(\widehat{\mathbf{z}}) > 0$ implies that the marginal distribution $p(\widehat{z}_j) > 0$ for all \widehat{z}_j . For $\widehat{\mathbf{c}}^{(1)}$, we have

$$p(\widehat{\mathbf{c}}^{(1)}) = \frac{p(\widehat{\mathbf{z}}, \widehat{\mathbf{c}}^{(1)})}{p(\widehat{\mathbf{z}})},$$

where both the numerator and denominator are derived by invertible functions $\mathbf{h}^{(q)}$ and γ , respectively. Hence, $p(\widehat{\mathbf{z}}, \widehat{\mathbf{c}}^{(1)}) > 0$ everywhere in its domain, which also means that $p(\widehat{\mathbf{c}}^{(1)}) > 0$ and $p(\widehat{c}_i^{(1)}) > 0$ everywhere. Then, we have

$$\frac{\partial [\mathbf{h}_P^{(1)}(\mathbf{x}^{(1)})]_i}{\partial \widehat{z}_j} = 0,$$

for all $i \in [D_1]$ and $j \in [D]$ by Lemma 1. Then, we have $\mathbf{J}_{21}^{(1)} = \mathbf{0}_{D_1 \times D} \mathbf{J}_{11}^{(1)} = \mathbf{0}_{D_1 \times D}$. Consequently, we have the following block diagonal form for $\mathbf{J}^{(1)}$, i.e.,

$$\mathbf{J}^{(1)} = \begin{bmatrix} \mathbf{J}_{11}^{(1)} & \mathbf{0}_{D \times D_1} \\ \mathbf{0}_{D_1 \times D} & \mathbf{J}_{22}^{(1)} \end{bmatrix}.$$

With invertibility of $\widehat{\mathbf{f}}^{(q)}$ and $\mathbf{g}^{(q)}$, we have

$$|\det \mathbf{J}^{(1)}| = |\det \mathbf{J}_{11}^{(1)}| |\det \mathbf{J}_{22}^{(1)}| \neq 0,$$

which implies that $\widehat{\mathbf{z}} = \gamma(\mathbf{z})$ and $\widehat{\mathbf{c}}^{(1)} = \delta^{(1)}(\mathbf{c}^{(1)})$ with invertible functions $\gamma(\cdot)$ and $\delta^{(1)}(\cdot)$. The similar proof technique applies to $\delta^{(2)}(\cdot)$. \square

C Proof of Theorem 2

Theorem 2. Under the generative model in (2) and Assumptions 1 and 2, assume that $(\mathbf{x}_\ell^{(1)}, \mathbf{x}_\ell^{(2)})$ for $\ell = 1, \dots, N$ are i.i.d. samples of $(\mathbf{x}^{(1)}, \mathbf{x}^{(2)})$. Denote $\widehat{\mathbf{f}}^{(q)} \in \mathcal{F}$ as any solution of (3) with the invertability constraint satisfied. Then, we have the following holds with probability of at least $1 - \delta$:

$$\mathbb{E} \left[\sum_{i=1}^D \sum_{j=1}^{D_q} (\partial [\widehat{\mathbf{f}}_s(\mathbf{x}^{(q)})]_i / \partial c_j^{(q)})^2 \right] = O \left(\left(D \mathfrak{R}_N + \sqrt{\log(1/\delta)/N} + \nu^2 \right)^{2/3} \right) \quad (\text{C.1})$$

for any $\mathbf{c}^{(q)} \in \mathcal{C}_q$ such that $-C_p + \kappa_j \leq c_j^{(q)} \leq C_p - \kappa_j$ for all $j \in [D_q]$ and all $i \in [D]$, where $\kappa_j = \Omega((3/C_d)^{1/3} (4C_f(2D\mathfrak{R}_N + C_f\sqrt{\log(1/\delta)/2N} + 4\nu^2)^{1/6})$.

C.1 A Lemma on Rademacher complexity

To derive the Rademacher complexity of the loss function, we have the following lemma

Lemma 2 Consider the following function class

$$\mathcal{H} = \left\{ l(\mathbf{x}^{(1)}, \mathbf{x}^{(2)}) \mid l(\mathbf{x}^{(1)}, \mathbf{x}^{(2)}) = \sum_{d=1}^D \left(\mathbf{f}_d^{(1)}(\mathbf{x}^{(1)}) - \mathbf{f}_d^{(2)}(\mathbf{x}^{(2)}) \right)^2 \right\}$$

where $\mathbf{f}_d^{(1)}, \mathbf{f}_d^{(2)} \in \mathcal{F}_d$ are as defined in Assumption 2. Assume that $\mathbf{f}_d^{(q)}(\mathbf{x}^{(q)}) \leq C_f$ for all $\mathbf{f}_d^{(q)} \in \mathcal{F}_d$, where $C_f > 0$. Then, the Rademacher complexity of class \mathcal{H} is bounded by

$$\mathfrak{R}_N(\mathcal{H}) \leq 4DC_f\mathfrak{R}_N.$$

Proof: First, we have the function $\left| \mathbf{f}_d^{(1)}(\mathbf{x}^{(1)}) - \mathbf{f}_d^{(2)}(\mathbf{x}^{(2)}) \right|$ bounded within $[0, 2C_f]$. According to the Lipschitz composition property of Rademacher complexity [48], we have

$$\mathfrak{R}_N(\phi \circ \mathcal{F}) \leq L_\phi \mathfrak{R}_N(\mathcal{F})$$

where L_ϕ is the Lipschitz constant of ϕ . Here $\phi(x) = x^2$ and $L_\phi = 4C_f$.

Combining the linearity property of the Rademacher complexity [48], we have

$$\mathfrak{R}_N(\mathcal{H}) \leq 4DC_f\mathfrak{R}_N \tag{C.2}$$

which completes the proof of the lemma. Note that (C.2) is derived by treating $\mathbf{f}_d^{(q)}$ for $d \in [D]$ as individual functions. However, $\mathbf{f}_d^{(q)}$ for $d \in [D]$ are the first D outputs of the same function $\mathbf{f}^{(q)}$ —which means that many parameters of these D functions are constrained to be identical. Nonetheless, this fact does not affect the inequality in (C.2) since adding confining constraints to the function class \mathcal{H} only reduces the Rademacher complexity [48]. \square

C.2 Proof of Theorem 2

First, we bound the true risk on the view matching loss. Consider the regression problem given $(\mathbf{x}_\ell^{(1)}, \mathbf{x}_\ell^{(2)})$ as samples, we have

$$\underset{\mathbf{f}^{(1)}, \mathbf{f}^{(2)}}{\text{minimize}} \frac{1}{N} \sum_{\ell=1}^N \left\| \mathbf{f}_S^{(1)}(\mathbf{x}_\ell^{(1)}) - \mathbf{f}_S^{(2)}(\mathbf{x}_\ell^{(2)}) \right\|_2^2.$$

By Lemma 2 and [49, Theorem 3.3], we have the following hold with probability at least $1 - \delta$

$$\begin{aligned} \mathbb{E} \left[\left\| \mathbf{f}_S^{(1)}(\mathbf{x}_\ell^{(1)}) - \mathbf{f}_S^{(2)}(\mathbf{x}_\ell^{(2)}) \right\|_2^2 \right] &\leq \frac{1}{N} \sum_{\ell=1}^N \left\| \mathbf{f}_S^{(1)}(\mathbf{x}_\ell^{(1)}) - \mathbf{f}_S^{(2)}(\mathbf{x}_\ell^{(2)}) \right\|_2^2 \\ &\quad + 2\mathfrak{R}_N(\mathcal{H}) + 4C_f^2 \sqrt{\frac{\log(1/\delta)}{2N}}. \end{aligned}$$

By Assumption 2c, the first term on the right hand side can be bounded as

$$\begin{aligned} &\frac{1}{N} \sum_{\ell=1}^N \left\| \mathbf{f}_S^{(1)}(\mathbf{x}_\ell^{(1)}) - \mathbf{f}_S^{(2)}(\mathbf{x}_\ell^{(2)}) \right\|_2^2 \\ &= \frac{1}{N} \sum_{\ell=1}^N \left\| \mathbf{f}_S^{(1)}(\mathbf{x}_\ell^{(1)}) - \mathbf{u}_S^{(1)}(\mathbf{x}_\ell^{(1)}) + \mathbf{u}_S^{(1)}(\mathbf{x}_\ell^{(1)}) - \mathbf{u}_S^{(2)}(\mathbf{x}_\ell^{(2)}) + \mathbf{u}_S^{(2)}(\mathbf{x}_\ell^{(2)}) - \mathbf{f}_S^{(2)}(\mathbf{x}_\ell^{(2)}) \right\|_2^2 \\ &\leq \frac{1}{N} \sum_{\ell=1}^N (\nu + \nu)^2 = 4\nu^2. \end{aligned}$$

where the first equality is because there exist $\mathbf{u}^{(1)} \in \mathcal{G}^{-1}$ and $\mathbf{u}^{(2)} \in \mathcal{G}^{-1}$ such that $\mathbf{u}_S^{(1)}(\mathbf{x}^{(1)}) = \mathbf{u}_S^{(2)}(\mathbf{x}^{(2)}) = \gamma(\mathbf{z})$ and the second inequality is by the triangle inequality.

Therefore, by plugging in $\mathfrak{R}_N(\mathcal{H})$ we have:

$$\mathbb{E} \left[\left\| \mathbf{f}_S^{(1)}(\mathbf{x}_\ell^{(1)}) - \mathbf{f}_S^{(2)}(\mathbf{x}_\ell^{(2)}) \right\|_2^2 \right] \leq \epsilon$$

with the definition

$$\begin{aligned} \epsilon &:= 4\nu^2 + 8DC_f\mathfrak{R}_N + 4C_f^2 \sqrt{\frac{\log(1/\delta)}{2N}} \\ &= 4C_f \left(2D\mathfrak{R}_N + C_f \sqrt{\frac{\log(1/\delta)}{2N}} \right) + 4\nu^2. \end{aligned}$$

Next, we use the bound of true risk to bound the energy of the entries of the Jacobian matrix on the left hand side of Eq. (C.1). Denote $\mathbf{h}_S^{(q)} = \mathbf{f}_S^{(q)} \circ \mathbf{g}^{(q)}$. We define the error for any individual sample pair $(\mathbf{x}_\ell^{(1)}, \mathbf{x}_\ell^{(2)}) \sim p(\mathbf{x}^{(1)}, \mathbf{x}^{(2)})$ as

$$\left\| \mathbf{f}_S^{(1)}(\mathbf{x}_\ell^{(1)}) - \mathbf{f}_S^{(2)}(\mathbf{x}_\ell^{(2)}) \right\|_2^2 = \varepsilon_\ell,$$

with $\mathbb{E}[\varepsilon_\ell] \leq \epsilon$.

Define another two pairs of samples, such that

$$\begin{aligned} \left\| \mathbf{h}_S^{(1)} \left(\begin{bmatrix} \mathbf{z}_\ell \\ \mathbf{c}_\ell^{(1)} + \Delta \mathbf{e}_j \end{bmatrix} \right) - \mathbf{h}_S^{(2)} \left(\begin{bmatrix} \mathbf{z}_\ell \\ \mathbf{c}_\ell^{(2)} \end{bmatrix} \right) \right\|_2^2 &= \varepsilon_{\hat{\ell}}, \\ \left\| \mathbf{h}_S^{(1)} \left(\begin{bmatrix} \mathbf{z}_\ell \\ \mathbf{c}_\ell^{(1)} - \Delta \mathbf{e}_j \end{bmatrix} \right) - \mathbf{h}_S^{(2)} \left(\begin{bmatrix} \mathbf{z}_\ell \\ \mathbf{c}_\ell^{(2)} \end{bmatrix} \right) \right\|_2^2 &= \varepsilon_{\tilde{\ell}}, \end{aligned}$$

where $\Delta > 0$ and \mathbf{e}_j is the unit vector in the $c_j^{(1)}$ direction. Then by triangle inequality we have

$$\left\| \mathbf{h}_S^{(1)} \left(\begin{bmatrix} \mathbf{z}_\ell \\ \mathbf{c}_\ell^{(1)} + \Delta \mathbf{e}_j \end{bmatrix} \right) - \mathbf{h}_S^{(1)} \left(\begin{bmatrix} \mathbf{z}_\ell \\ \mathbf{c}_\ell^{(1)} - \Delta \mathbf{e}_j \end{bmatrix} \right) \right\|_2 \leq \sqrt{\varepsilon_{\hat{\ell}}} + \sqrt{\varepsilon_{\tilde{\ell}}}.$$

Define

$$\psi_{ij}(c_j^{(1)}) := \left[\mathbf{h}_S^{(1)} \left(\left[\bar{\mathbf{z}}^\top, (\bar{c}_1^{(1)}, \dots, c_j^{(1)}, \dots, \bar{c}_{D_1}^{(1)})^\top \right] \right) \right]_i,$$

which is a scalar function of $c_j^{(1)}$ with fixed $\bar{\mathbf{z}}$ and $\bar{c}_k^{(1)}$ for $k \neq j$.

Then the element $\frac{\partial [\widehat{\mathbf{f}}_S(\mathbf{x}^{(1)})]_i}{\partial c_j^{(1)}}$ can be estimated using the central difference formula as

$$\begin{aligned} \left| \frac{\partial [\widehat{\mathbf{f}}_S(\mathbf{x}^{(1)})]_i}{\partial c_j^{(1)}} \right| &= \left| \frac{\left[\mathbf{h}_S^{(1)} \left(\begin{bmatrix} \mathbf{z}_\ell \\ \mathbf{c}_\ell^{(1)} + \Delta \mathbf{e}_j \end{bmatrix} \right) - \mathbf{h}_S^{(1)} \left(\begin{bmatrix} \mathbf{z}_\ell \\ \mathbf{c}_\ell^{(1)} - \Delta \mathbf{e}_j \end{bmatrix} \right) \right]_i}{2\Delta} - \frac{\Delta^2}{12} (\psi_{ij}'''(\xi_1) + \psi_{ij}'''(\xi_2)) \right| \\ &\leq \frac{\left| \left[\mathbf{h}_S^{(1)} \left(\begin{bmatrix} \mathbf{z}_\ell \\ \mathbf{c}_\ell^{(1)} + \Delta \mathbf{e}_j \end{bmatrix} \right) - \mathbf{h}_S^{(1)} \left(\begin{bmatrix} \mathbf{z}_\ell \\ \mathbf{c}_\ell^{(1)} - \Delta \mathbf{e}_j \end{bmatrix} \right) \right]_i \right|}{2\Delta} + \left| \frac{\Delta^2}{6} \psi_{ij}'''(\xi') \right|, \end{aligned}$$

where $\xi_1 \in (c_{\ell,j}^{(1)}, c_{\ell,j}^{(1)} + \Delta)$, $\xi_2 \in (c_{\ell,j}^{(1)} - \Delta, c_{\ell,j}^{(1)})$ and by intermediate value theorem $\xi' \in (c_{\ell,j}^{(1)} - \Delta, c_{\ell,j}^{(1)} + \Delta)$. Since $|x_i| \leq \|\mathbf{x}\|_\infty \leq \|\mathbf{x}\|_2$, we have

$$\left| \frac{\partial [\widehat{\mathbf{f}}_S(\mathbf{x}^{(1)})]_i}{\partial c_j^{(1)}} \right| \leq \frac{\sqrt{\varepsilon_{\widehat{\ell}}} + \sqrt{\varepsilon_{\bar{\ell}}}}{2\Delta} + \left| \frac{\Delta^2}{6} \psi_{ij}'''(\xi') \right|.$$

By taking expectation, we have

$$\begin{aligned} \mathbb{E} \left[\left| \frac{\partial [\widehat{\mathbf{f}}_S(\mathbf{x}^{(1)})]_i}{\partial c_j^{(1)}} \right| \right] &\leq \frac{\mathbb{E}[\sqrt{\varepsilon_{\widehat{\ell}}}] + \mathbb{E}[\sqrt{\varepsilon_{\bar{\ell}}}]}{2\Delta} + \left| \frac{\Delta^2}{6} \psi_{ij}'''(\xi') \right| \\ &\leq \frac{\sqrt{\varepsilon}}{\Delta} + \frac{\Delta^2}{6} |\psi_{ij}'''(\xi')|, \end{aligned}$$

where the second inequality is by Jensen's inequality

$$\mathbb{E}[\sqrt{\varepsilon_{\ell}}] \leq \sqrt{\mathbb{E}[\varepsilon_{\ell}]} \leq \sqrt{\varepsilon},$$

due to the concavity of \sqrt{x} .

We aim to find the smallest upper bound, i.e.,

$$\inf_{0 < \Delta < \min\{C_p + c_{\ell,j}^{(1)}, C_p - c_{\ell,j}^{(1)}\}} \frac{\sqrt{\varepsilon}}{\Delta} + \frac{\Delta^2}{6} |\psi_{ij}'''(\xi')|. \quad (\text{C.3})$$

Note that the function in (C.3) is convex and smooth. We have the minimizer

$$\Delta^* \in \left\{ \left(\frac{3\sqrt{\varepsilon}}{|\psi_{ij}'''(\xi')|} \right)^{1/3}, \min\{C_p + c_{\ell,j}^{(1)}, C_p - c_{\ell,j}^{(1)}\} \right\},$$

which gives us the minimum

$$\inf_{\Delta} \frac{\sqrt{\varepsilon}}{\Delta} + \frac{\Delta^2}{6} |\psi_{ij}'''(\xi')| \leq \min \left\{ \frac{3}{2} \left(\frac{|\psi_{ij}'''(\xi')|}{3} \right)^{1/3} \varepsilon^{1/3}, \frac{\sqrt{\varepsilon}}{\kappa_j} + \frac{\kappa_j^2}{6} |\psi_{ij}'''(\xi')| \right\}.$$

where $\kappa_j = \min\{C_p + c_{\ell,j}^{(1)}, C_p - c_{\ell,j}^{(1)}\}$.

If $\kappa_j \geq \left(\frac{3\sqrt{\varepsilon}}{|\psi_{ij}'''(\xi')|} \right)^{1/3}$, then we can bound

$$\mathbb{E} \left[\left| \frac{\partial [\widehat{\mathbf{f}}_S(\mathbf{x}^{(1)})]_i}{\partial c_j^{(1)}} \right| \right] \leq \frac{3}{2} \left(\frac{|\psi_{ij}'''(\xi')|}{3} \right)^{1/3} \varepsilon^{1/3}.$$

With fixed N , one can choose $\varepsilon = 4C_f \left(2D\mathfrak{R}_N + C_f \sqrt{\frac{\log(1/\delta)}{2N}} \right) + 4\nu^2$, which gives the following bound

$$\mathbb{E} \left[\left| \frac{\partial [\widehat{\mathbf{f}}_S(\mathbf{x}^{(1)})]_i}{\partial c_j^{(1)}} \right| \right] \leq \frac{3}{2} \left(\frac{C_d}{3} \right)^{1/3} \left(4C_f \left(2D\mathfrak{R}_N + C_f \sqrt{\frac{\log(1/\delta)}{2N}} \right) + 4\nu^2 \right)^{1/3},$$

if $\kappa_j \geq \left(\frac{3}{C_d} \right)^{1/3} \left(4C_f \left(2D\mathfrak{R}_N + C_f \sqrt{\frac{\log(1/\delta)}{2N}} \right) + 4\nu^2 \right)^{1/6}$.

Considering all i, j pairs, we have

$$\mathbb{E} \left[\sum_{i=1}^D \sum_{j=1}^{D_1} \left| \frac{\partial [\widehat{\mathbf{f}}_S(\mathbf{x}^{(1)})]_i}{\partial c_j^{(1)}} \right| \right] \leq \frac{3}{2} D D_1 \left(\frac{C_d}{3} \right)^{1/3} \left(4C_f \left(2D\mathfrak{R}_N + C_f \sqrt{\frac{\log(1/\delta)}{2N}} \right) + 4\nu^2 \right)^{1/3}.$$

Since $\|\cdot\|_2$ is upper bounded by $\|\cdot\|_1$, we have

$$\mathbb{E} \left[\sum_{i=1}^D \sum_{j=1}^{D_q} \left(\frac{\partial [\widehat{\mathbf{f}}_S(\mathbf{x}^{(q)})]_i}{\partial c_j^{(q)}} \right)^2 \right] \leq \frac{9}{4} D^2 D_1^2 \left(\frac{C_d}{3} \right)^{2/3} \left(4C_f \left(2D\mathfrak{R}_N + C_f \sqrt{\frac{\log(1/\delta)}{2N}} \right) + 4\nu^2 \right)^{2/3},$$

which completes the proof.

D Proof of Proposition 1

The claim can be proved by contradiction. Take $q = 1$ for example. Suppose that there exists two elements \widehat{z}_i and $\widehat{c}_j^{(1)}$ that are dependent but (6) is 0. Let

$$\phi_1 = \mathbf{e}_i^\top, \quad \tau_1 = \mathbf{e}_j^\top,$$

which are valid choices. Then, we have

$$\mathbb{C}\text{ov}[\phi_1(\widehat{\mathbf{z}})\tau_1(\widehat{\mathbf{c}}^{(1)})] = \mathbb{E}[\widehat{z}_i\widehat{c}_j^{(1)}] - \mathbb{E}[\widehat{z}_i]\mathbb{E}[\widehat{c}_j^{(1)}].$$

Note that by definition of independence, we have

$$\mathbb{E}[\widehat{z}_i\widehat{c}_j^{(1)}] = \mathbb{E}[\widehat{z}_i]\mathbb{E}[\widehat{c}_j^{(1)}] \iff \widehat{z}_i \perp\!\!\!\perp \widehat{c}_j^{(1)}.$$

Hence, z_i and z_j being dependent means that

$$\mathbb{E}[\widehat{z}_i\widehat{c}_j^{(1)}] - \mathbb{E}[\widehat{z}_i]\mathbb{E}[\widehat{c}_j^{(1)}] \neq 0.$$

Consequently, one can see that

$$\sup_{\phi_1, \tau_1} \mathbb{C}\text{ov}[\phi_1(\widehat{\mathbf{z}})\tau_1(\widehat{\mathbf{c}}^{(1)})] \geq \mathbb{C}\text{ov}[\phi_1(\widehat{\mathbf{z}})\tau_1(\widehat{\mathbf{c}}^{(1)})]_{\phi_1=\mathbf{e}_i^\top, \tau_1=\mathbf{e}_j^\top} = \mathbb{C}\text{ov}[\widehat{z}_i\widehat{c}_j^{(1)}] \neq 0.$$

The above is a contradiction to our assumption that holds.

On the other hand, if \widehat{z}_i and $\widehat{c}_j^{(1)}$ are independent for all $i \in [D]$ and $j \in [D_1]$, then we have

$$\mathbb{E}[\phi(\widehat{z}_i)\tau(\widehat{c}_j^{(1)})] - \mathbb{E}[\phi(\widehat{z}_i)]\mathbb{E}[\tau(\widehat{c}_j^{(1)})] = 0,$$

for all $i \in [D]$ and $j \in [D_1]$, for any $\phi : \mathbb{R} \rightarrow \mathbb{R}$ and $\tau : \mathbb{R} \rightarrow \mathbb{R}$.

E Detailed Algorithm Implementation

Recall that the proposed criterion is

$$\underset{\mathbf{f}^{(1)}, \mathbf{f}^{(2)}}{\text{maximize}} \text{Tr} \left(\frac{1}{N} \sum_{\ell=1}^N \mathbf{f}_S^{(1)}(\mathbf{x}_\ell^{(1)}) \mathbf{f}_S^{(2)}(\mathbf{x}_\ell^{(2)})^\top \right) \quad (\text{E.1a})$$

$$\text{subject to } \mathbf{f}^{(q)} \text{ for } q = 1, 2 \text{ are invertible,} \quad (\text{E.1b})$$

$$\frac{1}{N} \sum_{\ell=1}^N \mathbf{f}_S^{(q)}(\mathbf{x}_\ell^{(q)}) \mathbf{f}_S^{(q)}(\mathbf{x}_\ell^{(q)})^\top = \mathbf{I}, \quad \frac{1}{N} \sum_{\ell=1}^N \mathbf{f}_S^{(q)}(\mathbf{x}_\ell^{(q)}) = \mathbf{0}, \quad q = 1, 2, \quad (\text{E.1c})$$

$$\mathbf{f}_S^{(q)}(\mathbf{x}_\ell^{(q)}) \perp\!\!\!\perp \mathbf{f}_P^{(q)}(\mathbf{x}_\ell^{(q)}), \quad q = 1, 2, \quad (\text{E.1d})$$

We will use neural networks to parameterize the functions that we aim to learn. To move forward, first, as we have shown in the proof of Theorem 1, Eq. (E.1) is equivalent to the following:

$$\underset{\mathbf{f}^{(1)}, \mathbf{f}^{(2)}}{\text{minimize}} \frac{1}{N} \sum_{\ell=1}^N \left\| \mathbf{f}_S^{(1)}(\mathbf{x}_\ell^{(1)}) - \mathbf{f}_S^{(2)}(\mathbf{x}_\ell^{(2)}) \right\|_2^2 \quad (\text{E.2a})$$

$$\text{subject to } \frac{1}{N} \sum_{\ell=1}^N \mathbf{f}_S^{(q)}(\mathbf{x}_\ell^{(q)}) \mathbf{f}_S^{(q)}(\mathbf{x}_\ell^{(q)})^\top = \mathbf{I}, \quad \frac{1}{N} \sum_{\ell=1}^N \mathbf{f}_S^{(q)}(\mathbf{x}_\ell^{(q)}) = \mathbf{0}, \quad q = 1, 2 \quad (\text{E.2b})$$

$$\mathbf{f}^{(q)} \text{ for } q = 1, 2 \text{ are invertible}, \quad (\text{E.2c})$$

$$\mathbf{f}_S^{(q)}(\mathbf{x}_\ell^{(q)}) \perp\!\!\!\perp \mathbf{f}_P^{(q)}(\mathbf{x}_\ell^{(q)}), \quad q = 1, 2, \quad (\text{E.2d})$$

Note that we have manifold constraints on both neural networks $\mathbf{f}_S^{(1)}$ and $\mathbf{f}_S^{(2)}$. Directly optimizing over such manifold constraints may be costly and challenging. To reduce the difficulty of this constrained problem, we introduce a slack variable \mathbf{u}_ℓ and recast the formulation in (E.2) as follows:

$$\underset{\mathbf{f}^{(1)}, \mathbf{f}^{(2)}, \mathbf{u}_\ell}{\text{minimize}} \mathcal{L} = \frac{1}{N} \sum_{\ell=1}^N \mathcal{L}_\ell = \frac{1}{N} \sum_{\ell=1}^N \sum_{q=1}^2 \left\| \mathbf{u}_\ell - \mathbf{f}_S^{(q)}(\mathbf{x}_\ell^{(q)}) \right\|_2^2 \quad (\text{E.3a})$$

$$\text{subject to } \frac{1}{N} \sum_{\ell=1}^N \mathbf{u}_\ell \mathbf{u}_\ell^\top = \mathbf{I}, \quad \frac{1}{N} \sum_{\ell=1}^N \mathbf{u}_\ell = \mathbf{0}. \quad (\text{E.3b})$$

$$\mathbf{f}^{(q)} \text{ for } q = 1, 2 \text{ are invertible}, \quad (\text{E.3c})$$

$$\mathbf{f}_S^{(q)}(\mathbf{x}_\ell^{(q)}) \perp\!\!\!\perp \mathbf{f}_P^{(q)}(\mathbf{x}_\ell^{(q)}), \quad q = 1, 2, \quad (\text{E.3d})$$

Ideally, we hope that $\mathbf{u}_\ell = \gamma(\mathbf{z}_\ell)$. Introducing \mathbf{u}_ℓ makes the $\mathbf{f}^{(1)}$ and $\mathbf{f}^{(2)}$ subproblems unconstrained. This is a commonly used reformulation in neural network based multiview matching (see [21, 27]), which is reminiscent of the MAX-VAR formulation of CCA [23, 36, 37]. Such reformulations oftentimes make algorithm design easier, since the constraints are simplified.

The invertibility and independence constraints in (E.3c) and (E.3d) are also not straightforward to enforce. Instead of directly enforcing the invertibility constraint in (E.3c), we design a regularization term. Specifically, we use the idea of autoencoder that reconstructs the samples from their latent representations $\mathbf{f}^{(q)}(\mathbf{x}_\ell^{(q)})$. We define a regularizer

$$\mathcal{V} = \frac{1}{N} \sum_{\ell=1}^N \mathcal{V}_\ell = \frac{1}{N} \sum_{\ell=1}^N \sum_{q=1}^2 \left\| \mathbf{x}_\ell^{(q)} - \mathbf{r}^{(q)}(\mathbf{f}^{(q)}(\mathbf{x}_\ell^{(q)})) \right\|_2^2, \quad (\text{E.4})$$

as the reconstruction loss, where $\mathbf{r}^{(q)}$'s are the reconstruction neural networks. Note that the above term being zero does not necessarily indicate that the function $\mathbf{f}^{(q)}$ is invertible, since this term is only imposed on limited number of samples. But in practice, this idea is effective in learning invertible transformations—also see [16, 27].

To promote the statistical independence constraint in (E.3d), we use the designed independence regularizer, i.e.,

$$\sup_{\phi^{(q)}, \tau^{(q)}} \mathcal{R}^{(q)} = \sup_{\phi^{(q)}, \tau^{(q)}} \frac{|\text{Cov}[\phi^{(q)}(\hat{\mathbf{z}}) \tau^{(q)}(\hat{\mathbf{c}}^{(q)})]|}{\left(\sqrt{\mathbb{V}[\phi^{(q)}(\hat{\mathbf{z}})]} \sqrt{\mathbb{V}[\tau^{(q)}(\hat{\mathbf{c}}^{(q)})]} \right)}, \quad (\text{E.5})$$

where $\phi^{(q)}$ and $\tau^{(q)}$ are again represented by neural networks.

Let θ collect the parameters of $\mathbf{f}^{(q)}$ and $\mathbf{r}^{(q)}$, and η the parameters of $\phi^{(q)}$ and $\tau^{(q)}$. Putting all the terms together, our working cost function is summarized as follows:

$$\min_{\mathbf{U}, \boldsymbol{\theta}} \max_{\boldsymbol{\eta}} \frac{1}{N} \sum_{\ell=1}^N \mathcal{L}_{\ell}(\boldsymbol{\theta}, \mathbf{U}) + \beta \frac{1}{N} \sum_{\ell=1}^N \mathcal{V}_{\ell}(\boldsymbol{\theta}) + \lambda \mathcal{R}(\boldsymbol{\theta}, \boldsymbol{\eta}), \quad (\text{E.6a})$$

$$\text{subject to } \frac{1}{N} \sum_{\ell=1}^N \mathbf{U} \mathbf{U}^{\top} = \mathbf{I}, \quad \frac{1}{N} \mathbf{U} \mathbf{1} = \mathbf{0}, \quad (\text{E.6b})$$

where $\mathbf{U} = [\mathbf{u}_1, \dots, \mathbf{u}_N] \in \mathbb{R}^{D \times N}$, and β and λ are nonnegative and $\mathcal{R} = \sum_{q=1}^2 \mathcal{R}^{(q)}$.

In terms of algorithm design, we propose to handle \mathbf{U} , $\boldsymbol{\theta}$ and $\boldsymbol{\eta}$ cyclically when the other two are fixed, i.e., alternating optimization (AO).

First, we use stochastic gradient descent and ascent for the unconstrained $\boldsymbol{\theta}$ and $\boldsymbol{\eta}$ subproblems. To proceed, we sample a batch of data indexed by $\mathcal{B} \subseteq [N]$. Then, $\boldsymbol{\theta}$ and $\boldsymbol{\eta}$ can be updated by any stochastic gradient based optimizers, e.g., the plain-vanilla stochastic gradient descent/ascent,

$$\begin{aligned} \boldsymbol{\theta} &\leftarrow \boldsymbol{\theta} - \gamma \left(\frac{1}{|\mathcal{B}|} \sum_{\ell \in \mathcal{B}} (\nabla_{\boldsymbol{\theta}} \mathcal{L}_{\ell}(\boldsymbol{\theta}, \mathbf{U}) + \beta \nabla_{\boldsymbol{\theta}} \mathcal{V}_{\ell}(\boldsymbol{\theta})) + \lambda \widehat{\nabla}_{\boldsymbol{\theta}} \mathcal{R}(\boldsymbol{\theta}, \boldsymbol{\eta}) \right), \\ \boldsymbol{\eta} &\leftarrow \boldsymbol{\eta} + \delta \left(\lambda \widehat{\nabla}_{\boldsymbol{\eta}} \mathcal{R}(\boldsymbol{\theta}, \boldsymbol{\eta}) \right), \end{aligned}$$

where γ and δ are the step sizes for the updates of $\boldsymbol{\theta}$ and $\boldsymbol{\eta}$, respectively. The stochastic gradients of \mathcal{L} , \mathcal{V} are defined as follows:

$$\widehat{\nabla}_{\boldsymbol{\theta}} \mathcal{L} := \frac{1}{|\mathcal{B}|} \sum_{\ell \in \mathcal{B}} \nabla_{\boldsymbol{\theta}} \mathcal{L}_{\ell}(\boldsymbol{\theta}, \mathbf{U}) \quad (\text{E.7a})$$

$$\widehat{\nabla}_{\boldsymbol{\theta}} \mathcal{V} := \frac{1}{|\mathcal{B}|} \sum_{\ell \in \mathcal{B}} \nabla_{\boldsymbol{\theta}} \mathcal{V}_{\ell}(\boldsymbol{\theta}). \quad (\text{E.7b})$$

In addition, the terms $\widehat{\nabla}_{\boldsymbol{\theta}} \mathcal{R}$ and $\widehat{\nabla}_{\boldsymbol{\eta}} \mathcal{R}$ are defined similarly. Taking the latter as an example. We have $\widehat{\nabla}_{\boldsymbol{\eta}} \mathcal{R} = \sum_{q=1}^2 \widehat{\nabla}_{\boldsymbol{\eta}} \mathcal{R}^{(q)}$, and $\widehat{\nabla}_{\boldsymbol{\eta}} \mathcal{R}^{(q)}$ is estimated by taking gradient w.r.t. $\boldsymbol{\eta}$ of the following batch-estimated $\mathcal{R}^{(q)}$ (the same holds for $\widehat{\nabla}_{\boldsymbol{\theta}} \mathcal{R}$):

$$\mathcal{R}_{\mathcal{B}}^{(q)} := \quad (\text{E.8a})$$

$$\frac{\left| \frac{1}{|\mathcal{B}|} \sum_{\ell \in \mathcal{B}} \left(\phi^{(q)}(\widehat{\mathbf{z}}_{\ell}) - \frac{1}{|\mathcal{B}|} \sum_{\ell \in \mathcal{B}} \phi^{(q)}(\widehat{\mathbf{z}}_{\ell}) \right) \left(\boldsymbol{\tau}^{(q)}(\widehat{\mathbf{c}}_{\ell}^{(q)}) - \frac{1}{|\mathcal{B}|} \sum_{\ell \in \mathcal{B}} \boldsymbol{\tau}^{(q)}(\widehat{\mathbf{c}}_{\ell}^{(q)}) \right) \right|}{\sqrt{\frac{1}{|\mathcal{B}|} \sum_{\ell \in \mathcal{B}} \left(\phi^{(q)}(\widehat{\mathbf{z}}_{\ell}) - \frac{1}{|\mathcal{B}|} \sum_{\ell \in \mathcal{B}} \phi^{(q)}(\widehat{\mathbf{z}}_{\ell}) \right)^2} \sqrt{\frac{1}{|\mathcal{B}|} \sum_{\ell \in \mathcal{B}} \left(\boldsymbol{\tau}^{(q)}(\widehat{\mathbf{c}}_{\ell}^{(q)}) - \frac{1}{|\mathcal{B}|} \sum_{\ell \in \mathcal{B}} \boldsymbol{\tau}^{(q)}(\widehat{\mathbf{c}}_{\ell}^{(q)}) \right)^2}}$$

$$\widehat{\nabla}_{\boldsymbol{\eta}} \mathcal{R}^{(q)} := \nabla_{\boldsymbol{\eta}} \mathcal{R}_{\mathcal{B}}^{(q)} \quad (\text{E.8b})$$

$$\widehat{\nabla}_{\boldsymbol{\theta}} \mathcal{R}^{(q)} := \nabla_{\boldsymbol{\theta}} \mathcal{R}_{\mathcal{B}}^{(q)}. \quad (\text{E.8c})$$

It was shown in [50] that the correlation coefficient is computed using random samples of Gaussian variables, the estimator in (E.8a) for $\mathcal{R}^{(q)}$ is asymptotically unbiased. For other distributions, the estimation also works well in practice; see, e.g., DCCA based works in [16].

Consider more general stochastic optimizers, e.g., Adam [51] and Adagrad [52]. Then, the updates can be summarized as follows:

$$\boldsymbol{\theta} \leftarrow \text{SGD_optimizer} \left(\boldsymbol{\theta}, \widehat{\nabla}_{\boldsymbol{\theta}} \mathcal{L} + \beta \widehat{\nabla}_{\boldsymbol{\theta}} \mathcal{V} + \lambda \widehat{\nabla}_{\boldsymbol{\theta}} \mathcal{R} \right) \quad (\text{E.9})$$

$$\boldsymbol{\eta} \leftarrow \text{SGD_optimizer} \left(\boldsymbol{\eta}, -\widehat{\nabla}_{\boldsymbol{\eta}} \mathcal{R} \right). \quad (\text{E.10})$$

where (E.10) uses the negative stochastic gradient since it is an ascending step, while stochastic optimizers are by default descending the objective function.

The U subproblem consists of (E.3a) and (E.3b). It can be re-expressed as follows by expanding (E.3a):

$$\begin{aligned} & \frac{1}{N} \sum_{\ell=1}^N \sum_{q=1}^2 \left\| \mathbf{u}_\ell - \mathbf{f}_S^{(q)}(\mathbf{x}_\ell^{(q)}) \right\|_2^2 \\ &= \frac{1}{N} \sum_{\ell=1}^N \text{Tr} \left(2\mathbf{u}_\ell \mathbf{u}_\ell^\top - 2\mathbf{u}_\ell \left(\mathbf{f}_S^{(1)}(\mathbf{x}_\ell^{(1)}) + \mathbf{f}_S^{(2)}(\mathbf{x}_\ell^{(2)}) \right)^\top + \sum_{q=1}^2 \mathbf{f}_S^{(q)}(\mathbf{x}_\ell^{(q)}) \mathbf{f}_S^{(q)}(\mathbf{x}_\ell^{(q)})^\top \right). \end{aligned}$$

Note that the first term is a constant by (E.3b) and the last term does not involve \mathbf{u}_ℓ . Then, we rewrite the \mathbf{u}_ℓ subproblem as

$$\begin{aligned} & \underset{U}{\text{maximize}} \quad \text{Tr} \left(U \left(\mathbf{F}^{(1)} + \mathbf{F}^{(2)} \right) \right), \\ & \text{subject to} \quad \frac{1}{N} U U^\top = \mathbf{I}, \quad \frac{1}{N} U \mathbf{1} = \mathbf{0}, \end{aligned} \tag{E.11}$$

where $\mathbf{F}^{(q)} = \left[\mathbf{f}_S^{(q)}(\mathbf{x}_1^{(q)}), \dots, \mathbf{f}_S^{(q)}(\mathbf{x}_N^{(q)}) \right]$. This is an orthogonal projection onto the set of row zero-mean and orthogonal matrices. It is shown in [27, Lemma 1] that such a projection problem, although nonconvex, can be solved to optimality via a mean-removed singular value decomposition (SVD) procedure, i.e.,

$$U \leftarrow \sqrt{N} S T^\top, \quad \text{with } S D T^\top = \text{SVD} \left(\left(\mathbf{F}^{(1)} + \mathbf{F}^{(2)} \right) \mathbf{W} \right), \tag{E.12}$$

where $\mathbf{W} = \mathbf{I}_N - \frac{1}{N} \mathbf{1} \mathbf{1}^\top$ removes the mean of $\mathbf{F}^{(1)} + \mathbf{F}^{(2)}$, $\mathbf{D} \in \mathbb{R}^{D \times D}$ holds the singular values, $\mathbf{S} \in \mathbb{R}^{D \times D}$ and $\mathbf{T} \in \mathbb{R}^{N \times D}$ are the left and right orthogonal matrices in the SVD, respectively.

To summarize, an alternating optimization algorithm is summarized in Algorithm 1. Notice that we use two different batch sizes (denoted as \mathcal{B}_1 and \mathcal{B}_2 in line 4 of Algorithm 1) to construct the gradient estimations for $\widehat{\nabla}_\theta \mathcal{L}$, $\widehat{\nabla}_\theta \mathcal{V}$ and $\widehat{\nabla}_\eta \mathcal{R}$, $\widehat{\nabla}_\eta \mathcal{R}$, respectively. The reason is that accurately estimating of \mathcal{R} using (E.8a) often requires a relatively large batch size, while small batches may suffice for the gradient estimations of \mathcal{L} and \mathcal{V} , according to our extensive simulations.

Algorithm 1: Proposed Algorithm.

Data: $\mathbf{x}_\ell^{(q)}$ for $\ell = 1, \dots, N$ and $q = 1, 2$
Result: $\boldsymbol{\theta}^{(q)}$, $\boldsymbol{\eta}^{(q)}$

```

1 while stopping criterion is not reached do
2    $U \leftarrow \sqrt{N} S T^\top$  with  $S D T^\top = \text{SVD} \left( \left( \mathbf{F}^{(1)} + \mathbf{F}^{(2)} \right) \mathbf{W} \right)$ ;
3   while stopping criterion is not reached do
4     draw a random batch  $\mathcal{B}_1$  and  $\mathcal{B}_2$ ; // use  $|\mathcal{B}_2| > |\mathcal{B}_1|$ 
5      $\widehat{\nabla}_\theta \mathcal{L} \leftarrow \frac{1}{|\mathcal{B}_1|} \sum_{\ell \in \mathcal{B}_1} \nabla_\theta \mathcal{L}_\ell$ ;
6      $\widehat{\nabla}_\theta \mathcal{V} \leftarrow \frac{1}{|\mathcal{B}_1|} \sum_{\ell \in \mathcal{B}_1} \nabla_\theta \mathcal{V}_\ell$ ;
7      $\widehat{\nabla}_\eta \mathcal{R} \leftarrow \sum_{q=1}^2 \nabla_\eta \mathcal{R}_{\mathcal{B}_2}^{(q)}$ ; // using  $\mathcal{B}_2$  and (E.8a), (E.8b)
8      $\widehat{\nabla}_\theta \mathcal{R} \leftarrow \sum_{q=1}^2 \nabla_\theta \mathcal{R}_{\mathcal{B}_2}^{(q)}$ ; // using  $\mathcal{B}_2$  and (E.8a), (E.8c)
9      $\boldsymbol{\theta} \leftarrow \text{SGD\_optimizer} \left( \boldsymbol{\theta}, \widehat{\nabla}_\theta \mathcal{L} + \beta \widehat{\nabla}_\theta \mathcal{V} + \lambda \widehat{\nabla}_\theta \mathcal{R} \right)$ ; // descent
10     $\boldsymbol{\eta} \leftarrow \text{SGD\_optimizer} \left( \boldsymbol{\eta}, -\lambda \widehat{\nabla}_\eta \mathcal{R} \right)$ ; // ascent
11  end
12 end

```

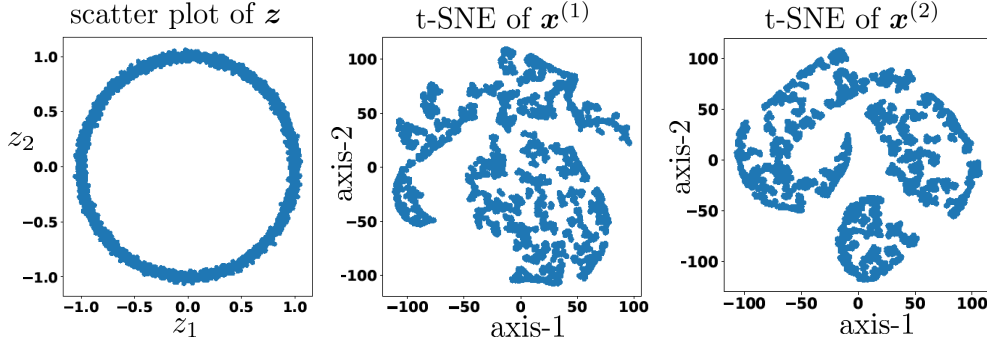


Figure F.1: Left: z ; middle: t-SNE of $x^{(1)}$; right: t-SNE of $x^{(2)}$.

F Experiments: More Details and Additional Real Data Set

In this section, we show all the experiment results with greater details, e.g., results under more metrics, more setting details, and more demonstrations. We also include one more real data experiment using the dSprites data [39].

F.1 Synthetic Data - More Details

In this subsection, we describe our synthetic experiments with richer details. For synthetic data, we generate the shared $z \in \mathbb{R}^2$ that is uniformly drawn from the unit circle, with noise $\mathcal{N}(0, 0.02^2)$ added to each dimension. The private components are scalars $c^{(1)} \sim \mathcal{N}(0, 2.0)$ and $c^{(2)} \sim \text{Laplace}(0, 4.0)$. The shared-to-private energy ratios for the two views are approximately -6 dB and -18 dB. The sample size is $N = 5,000$. And we use two different one-hidden-layer neural networks with 3 neurons and softplus activation to represent the invertible $g^{(q)}$'s. The network parameters are drawn from standard normal distribution.

The shared component z and the t-SNE of $x^{(1)}$ and $x^{(2)}$ are shown in Fig. F.1. One can see that by incorporating strong noise and nonlinear transformations, the shape of circle is hardly to be identified in both views.

In our simulations, $f^{(q)}$ is represented by a three-hidden-layer multi-layer perceptrons (MLPs) with 256 neurons in each layer with ReLU activations. In addition, $\phi^{(q)}$ and $\tau^{(q)}$ are represented by two-hidden-layer MLPs with 128 neurons in each layer. We set batch size to be 1000, $\beta = 1.0$, $\lambda = 0.1$. We use the Adam optimizer [51] with initial learning rate 0.001 for all the parameters. Besides, we also regularize the network parameters using $\|\eta\|_2^2$ with a regularization parameter 0.1. This often helps improve numerical stability when optimizing cost functions involving neural networks. We run lines 4-10 of Algorithm 1 for 10 epochs to update θ and η .

For ablation study, we test the methods with different combinations of \mathcal{L} , \mathcal{R} and \mathcal{V} , i.e.,

- (i) the proposed method ($\mathcal{L} + \mathcal{V} + \mathcal{R}$);
- (ii) the proposed without independence regularization ($\mathcal{L} + \mathcal{V}$);
- (iii) the proposed without reconstruction ($\mathcal{L} + \mathcal{R}$);
- (iv) the proposed with only latent correlation maximization (\mathcal{L});
- (v) we also test the performance with HSIC [34] as the independence regularizer ($\mathcal{L} + \mathcal{V} + \text{HSIC}$);
- (vi) in addition, we employ a baseline that uses the objective function of Barlow Twins [19] (BT-Loss).

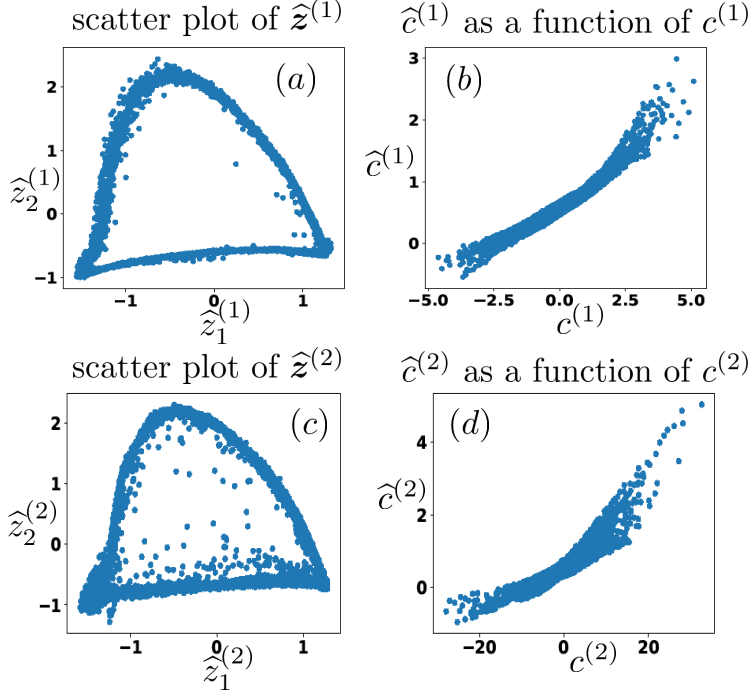


Figure F.2: (a) Scatter plot of $\hat{z}^{(1)}$; (b) $\hat{c}^{(1)}$ as a function of $c^{(1)}$; (c) Scatter plot of $\hat{z}^{(2)}$; (d) $\hat{c}^{(2)}$ as a function of $c^{(2)}$.

All methods stop when the average matching loss \mathcal{L} reaches 0.01, except that BT-LOSS stops when its loss reaches 0.001.

The learned components by the proposed method are shown in Fig. F.2. One can see that the estimated shared components are matched, while the second view exhibits relatively large noise level as expected. For the estimated private components, one can see that both $\delta^{(1)}(\cdot)$ and $\delta^{(2)}(\cdot)$ are approximately invertible functions.

In addition to using MINE as the mutual information (MI) estimator for performance evaluation, we also present the results that use the Gaussian kernel density estimation (KDE) [53] for MI value computation.

Table F.1 shows the results, with all the entries averaged over 10 random trials. One can see that the results via the Gaussian KDE are consistent with those under MINE. That is, the proposed $\mathcal{L} + \mathcal{V} + \mathcal{R}$ exhibits the best performance in terms of extracting and disentangling the shared and private information.

F.2 Synthetic Data - Additional Experiment

In this subsection, we demonstrate the performance of the proposed method under different levels of private component energy (which are often considered interference) [12, 13, 27]. First, we define the *shared-to-private ratio* (SPR) for the q -th view as

$$\text{SPR} = 10 \log_{10} \left(\frac{\frac{1}{DN} \sum_{\ell=1}^N \|z_{\ell}\|_2^2}{\frac{1}{D_q N} \sum_{\ell=1}^N \|c_{\ell}^{(q)}\|_2^2} \right) \text{ dB}.$$

For the experiment, we make both views have identical SPRs. We test the performance under SPR=-10 dB, -20 dB and -30 dB, respectively.

Table F.2 shows the evaluation results averaged from 10 trials. One can see that as SPR decreases, the MI between the extracted \hat{z} and z decreases—but only gracefully. The slight decline of performance is

Table F.1: Mutual information (MI) between groups of variables. “ \uparrow ”: high score preferred; “ \downarrow ”: low score preferred; “n/a”: not applicable; $\hat{z}^{(q)} = \hat{f}_S^{(q)}$ for $q = 1, 2$.

	$\hat{z}^{(1)}, z (\uparrow)$	$\hat{z}^{(2)}, z (\uparrow)$	$\hat{z}^{(1)}, c^{(1)} (\downarrow)$	$\hat{z}^{(2)}, c^{(2)} (\downarrow)$	$\hat{c}^{(1)}, c^{(1)} (\uparrow)$	$\hat{c}^{(2)}, c^{(2)} (\uparrow)$	$\hat{c}^{(1)}, z (\downarrow)$	$\hat{c}^{(2)}, z (\downarrow)$
Metric	MINE-based MI Estimation [43]							
\mathcal{L}	2.32±0.06	2.36±0.10	0.01±0.00	0.00±0.00	0.45±0.13	0.33±0.07	0.39±0.14	0.43±0.04
$\mathcal{L} + \mathcal{V}$	2.37±0.05	2.38±0.08	0.01±0.00	0.01±0.00	0.55±0.09	0.33±0.08	0.31±0.06	0.43±0.05
$\mathcal{L} + \mathcal{R}$	2.32±0.05	2.33±0.07	0.02±0.01	0.00±0.00	0.90±0.42	0.22±0.12	0.09±0.06	0.22±0.12
$\mathcal{L} + \mathcal{V} + \mathcal{R}$	2.43±0.04	2.39±0.09	0.01±0.01	0.01±0.00	1.22± 0.33	0.85±0.23	0.04±0.02	0.11±0.03
$\mathcal{L} + \mathcal{V} + \text{HSIC}$	2.48±0.09	2.43±0.08	0.01±0.00	0.01±0.01	0.68±0.25	0.52±0.14	0.04±0.01	0.07±0.02
BT-LOSS	0.53±0.20	0.42±0.20	0.00±0.00	0.00±0.00	n/a	n/a	n/a	n/a
Metric	Gaussian kernel density estimate (KDE)-based MI Estimation							
\mathcal{L}	2.73±0.22	2.88±0.22	0.00±0.00	0.00	0.33±0.13	0.01±0.02	0.34±0.13	0.37±0.06
$\mathcal{L} + \mathcal{V}$	2.95±0.21	2.91±0.26	0.00±0.01	0.00	0.38±0.11	0.01±0.02	0.24±0.04	0.39±0.07
$\mathcal{L} + \mathcal{R}$	2.83±0.18	2.86±0.15	0.00	0.00	0.72±0.40	0.10±0.10	0.08±0.07	0.28±0.16
$\mathcal{L} + \mathcal{V} + \mathcal{R}$	3.27±0.07	2.88±0.25	0.00±0.01	0.00	0.99±0.30	0.35±0.11	0.03±0.04	0.08±0.03
$\mathcal{L} + \mathcal{V} + \text{HSIC}$	3.35±0.16	2.95±0.33	0.00	0.00	0.78±0.22	0.06±0.06	0.05±0.02	0.02±0.01
BT-LOSS	1.17±0.37	1.37±0.27	0.02±0.02	0.00	n/a	n/a	n/a	n/a

Table F.2: Mutual information (MI) between groups of variables under different SPR. “ \uparrow ”: high score preferred; “ \downarrow ”: low score preferred; $\hat{z}^{(q)} = \hat{f}_S^{(q)}$ for $q = 1, 2$.

	$\hat{z}^{(1)}, z (\uparrow)$	$\hat{z}^{(2)}, z (\uparrow)$	$\hat{z}^{(1)}, c^{(1)} (\downarrow)$	$\hat{z}^{(2)}, c^{(2)} (\downarrow)$	$\hat{c}^{(1)}, c^{(1)} (\uparrow)$	$\hat{c}^{(2)}, c^{(2)} (\uparrow)$	$\hat{c}^{(1)}, z (\downarrow)$	$\hat{c}^{(2)}, z (\downarrow)$
SPR	MINE-based MI Estimation [43]							
-10 dB	2.41±0.07	2.43±0.05	0.01±0.01	0.01±0.01	1.72±0.41	0.52±0.10	0.02±0.01	0.19±0.03
-20 dB	1.81±0.10	2.15±0.09	0.10±0.06	0.01±0.01	1.41±0.15	1.15±0.07	0.08±0.04	0.06±0.02
-30 dB	1.16±0.07	1.55±0.10	0.11±0.09	0.07±0.04	1.77±0.42	0.73±0.14	0.03±0.02	0.14±0.11

because the matching of two views becomes harder when the private components get stronger. However, even if SPR=-30 dB, the extraction and disentanglement of private and shared information are still clearly achieved. Such robustness to strong private interference is considered a key feature of linear CCA [13] and post-nonlinear CCA [27]. Our analysis and evaluation in this work show that such resilience is also inherited by the proposed approach.

F.3 Real Data - More Details on Cars3D

In this subsection, we provide more detailed settings and results of the Cars3D experiment. To create a multiview dataset, we assume that given the car type that is captured by shared variables z and the azimuths that are captured by $c^{(q)}$, the generation mappings $g^{(1)}$ and $g^{(2)}$ produce car images with low elevations and high elevations, respectively (so they must be different mappings).

We split the car images as follows. We treat the same car model (e.g., a red convertible) with lower and higher elevations as $x_\ell^{(1)}$ and $x_\ell^{(2)}$, respectively. The azimuths are randomly shuffled with different pairs of $x_\ell^{(1)}$ and $x_\ell^{(2)}$. This way, if our generative model holds, z , $c^{(q)}$ and $g^{(q)}$ are responsible for ‘type’, ‘azimuth’ and ‘elevation’, respectively. Some samples are shown in Fig. F.3.

Under our splitting, each view has $2 \times 183 \times 24 = 8784$ RGB images that all have a size of $64 \times 64 \times 3$. We model the ‘type’ information z using $D = 10$ latent dimensions since many different factors (e.g., color and shape) together give rise to a ‘type’. On the other hand, we set $D_1 = D_2 = 2$ to model the ‘azimuth’ information.

Table F.3 shows network structures for the encoders and decoders of our formulation in (E.6). In the table, FC denotes fully connected layer, Conv denotes convolutional layer and Conv_Trans denotes 2D transposed

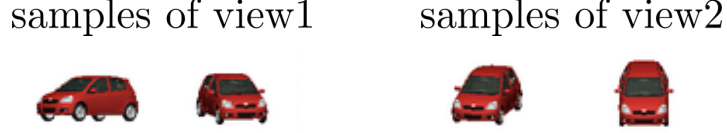


Figure F.3: Samples of the lower elevations (view1) and higher elevations (view2).

Table F.3: Network structures for the Cars3D experiment.

Encoders	Decoders
input: $\mathbf{x}_\ell^{(q)} \in \mathbb{R}^{64 \times 64 \times 3}$	input: $\mathbf{f}^{(q)}(\mathbf{x}_\ell^{(q)}) \in \mathbb{R}^{10+2}$
4 × 4 Conv, 32 ReLU, stride 2	FC 256, ReLU
4 × 4 Conv, 32 ReLU, stride 2	FC 4 × 4 × 64, ReLU
4 × 4 Conv, 64 ReLU, stride 2	4 × 4 Conv_Trans, 64 ReLU, stride 2
4 × 4 Conv, 64 ReLU, stride 2	4 × 4 Conv_Trans, 32 ReLU, stride 2
FC 256, ReLU	4 × 4 Conv_Trans, 32 ReLU, stride 2
FC 10+2	4 × 4 Conv_Trans, 3, stride 2

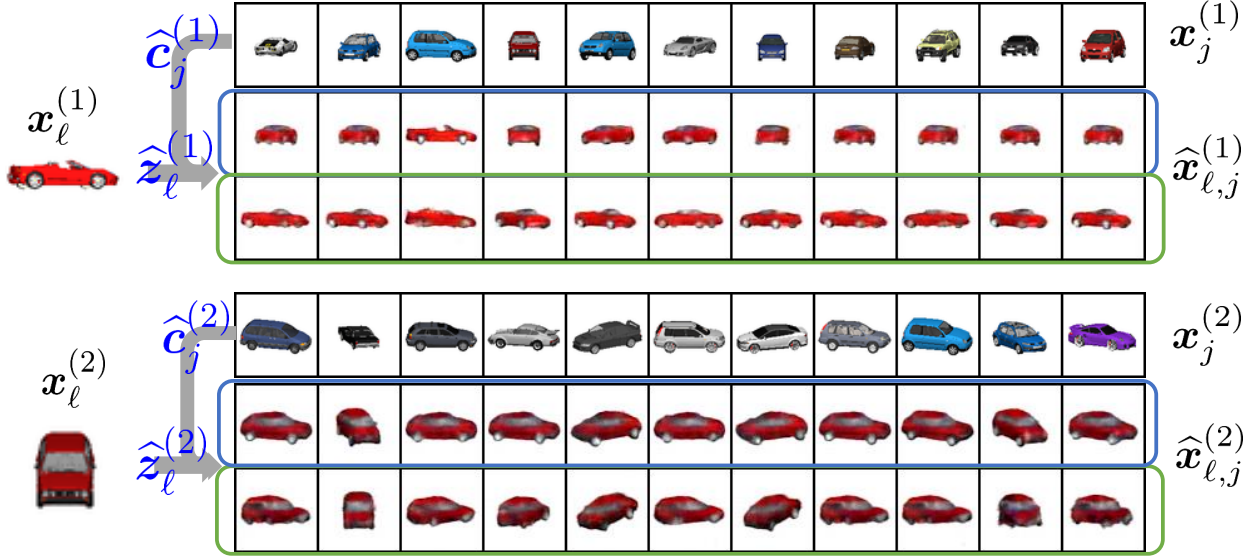


Figure F.4: Generated samples by fixing $\hat{\mathbf{z}}_\ell$ and varying $\hat{\mathbf{c}}_j^{(q)}$; rows in blue boxes are w/ \mathcal{R} ; rows in green boxes are w/o \mathcal{R} .

convolutional layer. As before, the structures of $\phi^{(q)}$ and $\tau^{(q)}$ are MLPs with two-hidden-layer and 256 neurons for each layer. For hyperparameters, we set batch size to be $|\mathcal{B}_1| = 100$ and $|\mathcal{B}_2| = 800$, $\beta = 0.1$, $\lambda = 1.0$. For this real data experiment, we also use Adam [51] as the optimizer with initial learning rate 0.001 for θ and 1.0 for η . We add $\|\eta\|_2^2$ for regularization with parameter 0.0001. We limit the inner loops for solving the θ and η subproblems to 10 epochs as well.

Figs. F.4 and F.5 show more results under the same setting as in Fig. 3 in the main text.

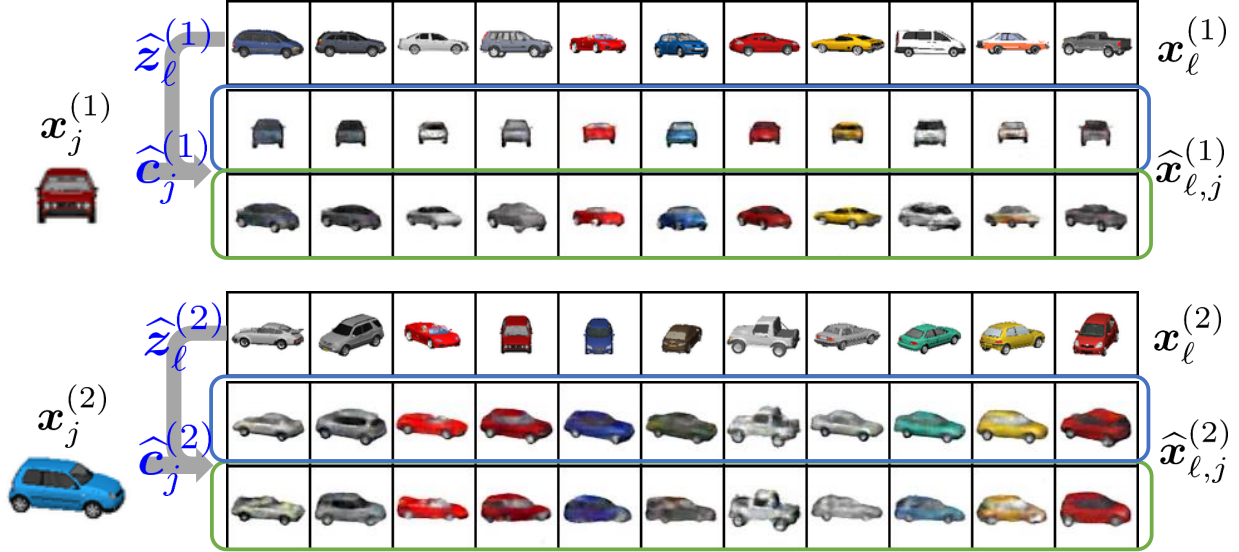


Figure F.5: Generated samples by fixing $\hat{c}_j^{(q)}$ and varying \hat{z}_l ; rows in blue boxes are w/ \mathcal{R} ; rows in green boxes are w/o \mathcal{R} .

F.4 Real Data - Additional Experiment on dSprites

In this subsection, we present the results on an additional dataset, i.e., dSprites [39].

In the dSprites dataset, 64×64 images are generated based on five factors: 3 shapes (square, ellipse, heart), 6 scales, 40 orientations, and 32 different horizontal and vertical coordinates.

In particular, we take a subset that contains squares and hearts as the two views of data. In this subset, all the data samples are with the same scale. We assume the generating functions $g^{(1)}$ and $g^{(2)}$ are responsible for the shape of square and heart, respectively. We treat the orientation and horizontal positions as the shared information, i.e., z , and the vertical position as the private information $c^{(q)}$. The vertical coordinates are random and not matched between different pairs of $x_\ell^{(1)}$ and $x_\ell^{(2)}$. Overall, we have 40,960 samples for each view. We set $D = 2$ and $D_1 = D_2 = 1$.

We use the same neural network structure as in Table F.3. The only differences lie in the input and latent dimensions. The network structure for $\phi^{(q)}$ and $\tau^{(q)}$ are MLPs with two hidden layers of 128 neurons, and we set $|\mathcal{B}_1| = 100$, $|\mathcal{B}_2| = 500$, $\beta = 0.1$, and $\lambda = 100.0$. Similar as before, we use the Adam [51] optimizer with initial learning rate 0.001 for θ . As before, we add a squared ℓ_2 norm regularization on the network parameters η , and set the regularization parameter to 0.1. We let the inner loop stochastic optimizers run for 10 epochs.

Fig. F.6 shows the results. We follow the same idea of evaluation as in Car3D. To be specific, we extract $\hat{z}_\ell^{(q)} = \hat{f}_S(x_\ell^{(q)})$ that represents the rotation and horizontal coordinate information and $\hat{c}_j^{(q)} = \hat{f}_P(x_\ell^{(q)})$. And we combine this information together to generate synthetic samples $\hat{x}_{\ell,j}^{(q)}$ with the learned reconstruction network $r^{(q)}$, i.e., $\hat{x}_{\ell,j}^{(q)} = \hat{r}^{(q)}([\hat{z}_\ell^{(q)\top}, (\hat{c}_j^{(q)})^\top]^\top)$.

The observations are similar to what we have seen in the Car3D experiments. One can see that without using the independence regularizer, the generated samples may have rotation change, shape deformation compared to $x_\ell^{(q)}$ or simply the Y information is not exactly replicated from the sample $x_j^{(q)}$.

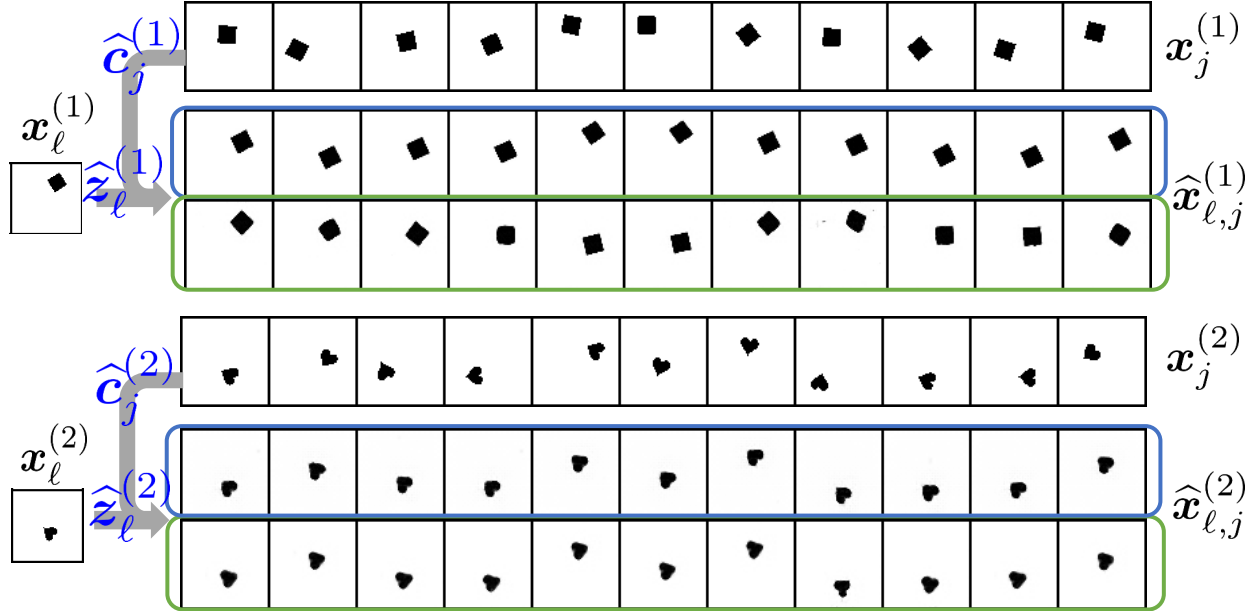


Figure F.6: Generated samples by fixing \hat{z}_ℓ (rotation and horizontal position) and varying $\hat{c}_j^{(q)}$ (vertical position). Top: the square view; bottom: the heart view; rows in blue boxes are w/ \mathcal{R} ; rows in green boxes are w/o \mathcal{R}

F.5 Real Data - More Details and Evaluations on Two-View MNIST

In this subsection, we provide more details and evaluation results on the MNIST experiment. The way of generating such two views (as shown in Fig. 4 of the main text) of MNIST data is similar to the data augmentation ideas used in AM-SSL, e.g., rotation, adding noise, cropping, flipping [4, 17]. We aim to match the two views and try to learn the shared representations, which should encode the class label information. The dataset has 70,000 samples that are 28×28 images of handwritten digits. For the latent dimension, we set $D = 10$, $D_1 = 20$ and $D_2 = 50$. In particular, since the second view consists of large random noise that are not of interest, we only add the independence regularizer $\mathcal{R}^{(1)}$ on the first view (i.e., the rotated digits) to learn the private component of $x_\ell^{(1)}$. The learned $\hat{c}_\ell^{(1)}$ was used to generate new samples; see the illustration in our main text.

The network structure used for all methods is shown in Table F.4. The network structure for $\phi^{(a)}$ and $\tau^{(a)}$ are MLPs with three hidden layers of 64 neurons. For hyperparameters, we set batch size to be $|\mathcal{B}_1| = 100$ and $|\mathcal{B}_2| = 1000$, $\beta = 1.0$, $\lambda = 100.0$. For optimizer, we also use Adam [51] with initial learning rate 0.001 for θ and 1.0 for η . And we add squared ℓ_2 regularization for both θ and η , with different regularization parameters that are 0.0001 and 0.1, respectively. We also run the SGD optimizer for 10 epochs to update θ and η .

In Table F.5, we show more evaluation results on the learned shared information across views. To be specific, we feed the learned $\hat{z}_\ell^{(1)}$'s to a classifier and the k -means algorithm, to observe if the learned representations improve the performance of supervised and unsupervised learning tasks. For the classification task, we split the data as 50,000/10,000/10,000 for training/validation/test sets. We train a linear support vector machine (SVM) using the training data. The performance is measured by classification error (ERR). For the clustering task, we use the standard k -means to cluster on all the data samples. After clustering, we report the performance on the test set. We use a number of metrics to measure performance, namely, clustering accuracy (ACC), normalized mutual information (NMI), and adjusted Rand index (ARI) [54].

Table F.4: Network structures for the MNIST experiment.

Encoders	Decoders
input: $\mathbf{x}_\ell^{(q)} \in \mathbb{R}^{28 \times 28 \times 1}$	input: $\mathbf{f}^{(q)}(\mathbf{x}_\ell^{(q)}) \in \mathbb{R}^{D+D_q}$
4×4 Conv, 64 ReLU, stride 2	FC 256, ReLU
4×4 Conv, 32 ReLU, stride 2	FC $7 \times 7 \times 32$, ReLU
FC 256, ReLU	4×4 Conv_Trans, 64 ReLU, stride 2
FC $D + D_q$	4×4 Conv_Trans, 1, stride 2

Table F.5: The classification error (first row) and clustering results (rows 2 to 4) of the two-view MNIST dataset. “ \uparrow ”: high score preferred; “ \downarrow ”: low score preferred.

	Baseline	$\mathcal{L} + \mathcal{V} + \mathcal{R}$	$\mathcal{L} + \mathcal{V}$	DCCA	DCCAE	BT-loss
ERR (\downarrow)	13.40%	2.81% \pm 0.21%	2.95% \pm 0.23%	2.87% \pm 0.16%	2.85% \pm 0.05%	2.05% \pm 0.07%
ACC (\uparrow)	37.35%	97.03% \pm 0.13%	96.80% \pm 0.40%	97.02% \pm 0.12%	96.95% \pm 0.12%	98.06% \pm 0.06%
NMI (\uparrow)	0.337	0.922 \pm 0.003	0.923 \pm 0.007	0.922% \pm 0.003	0.920 \pm 0.003	0.947 \pm 0.002
ARI (\uparrow)	0.216	0.936 \pm 0.003	0.931 \pm 0.009	0.935% \pm 0.003	0.934 \pm 0.002	0.958 \pm 0.001

Among these metrics, ARI ranges from -1 to $+1$, with 1 being the best and -1 the worst and NMI range from 0 to 1 with 1 being the best.

The “Baseline” denotes the results of simply applying SVM and k -means onto the raw data of the first view, i.e., $\mathbf{x}_\ell^{(1)}$ for $\ell = 1, \dots, N$. All the results of algorithms that involve stochastic methods are averaged over 5 random initializations. One can see that all methods have comparably good results in terms of learning informative representations across views. The results empirically validate our Theorem 1(i) that latent correlation maximization is a useful criterion to extract the shared information with guarantees. In particular, BT-loss performs slightly better in terms of benefiting downstream classification and clustering tasks. Nonetheless, the proposed method can also guarantee extracting private information and facilitate cross-view image generation (see the experiments in the main text), which is out the reach of BT-loss.